Our present understanding of the $^{3}He(\alpha,\gamma)^{7}Be$ key astrophysical nuclear reaction

Inaugural workshop on Nuclear Astrochemistry

ECT, Trento, Italy, 26 February - 1 March 2024*

Tamás Szücs

HUN REN | atomki DEBRECEN

BBN and solar pp-chain

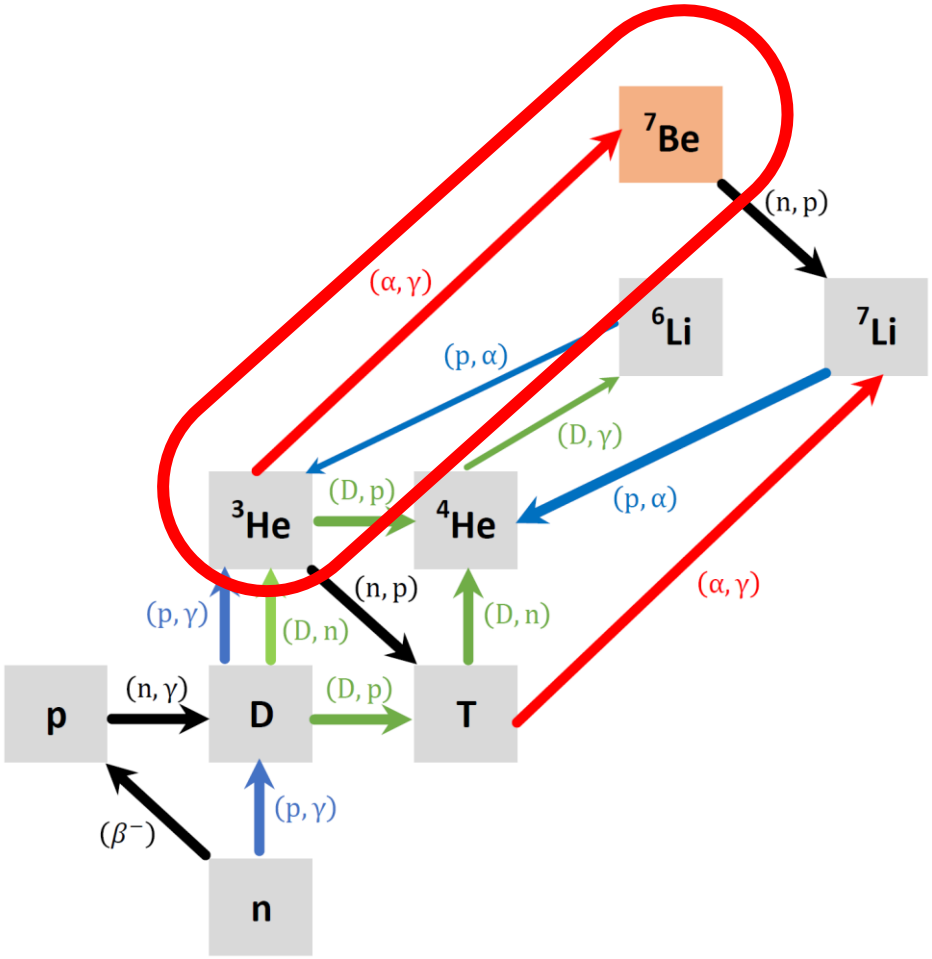

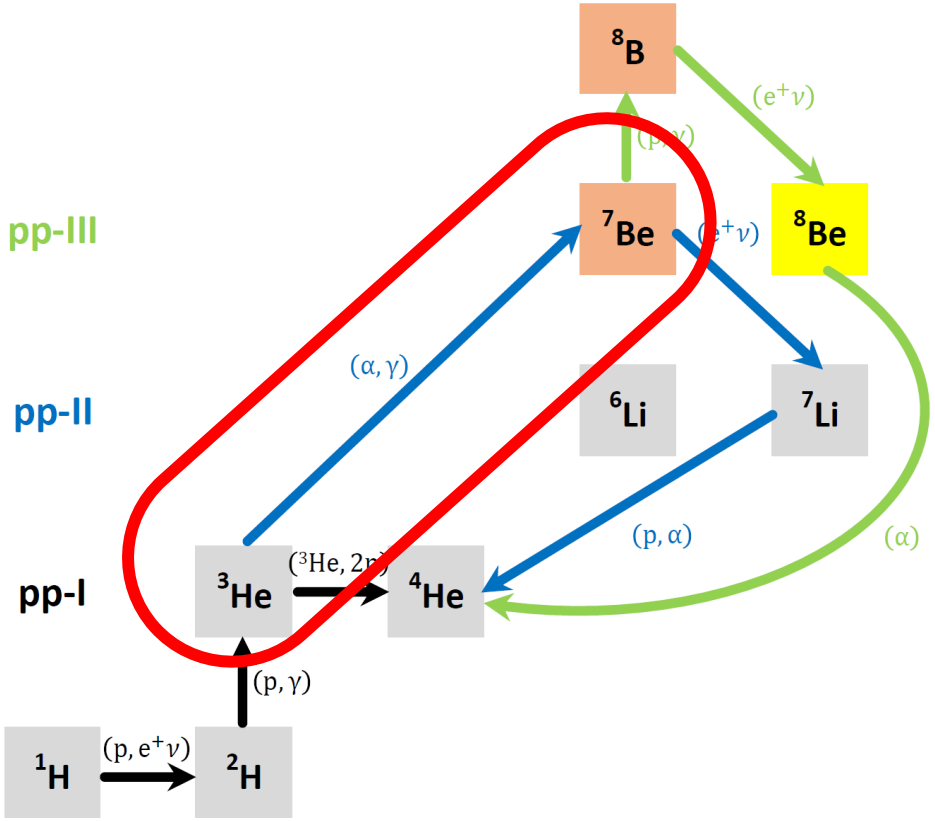

Tamás Szücs | tszucs@atomki.hu | 27.02.2024

Primordial Li problem and the neutrinos from SSM

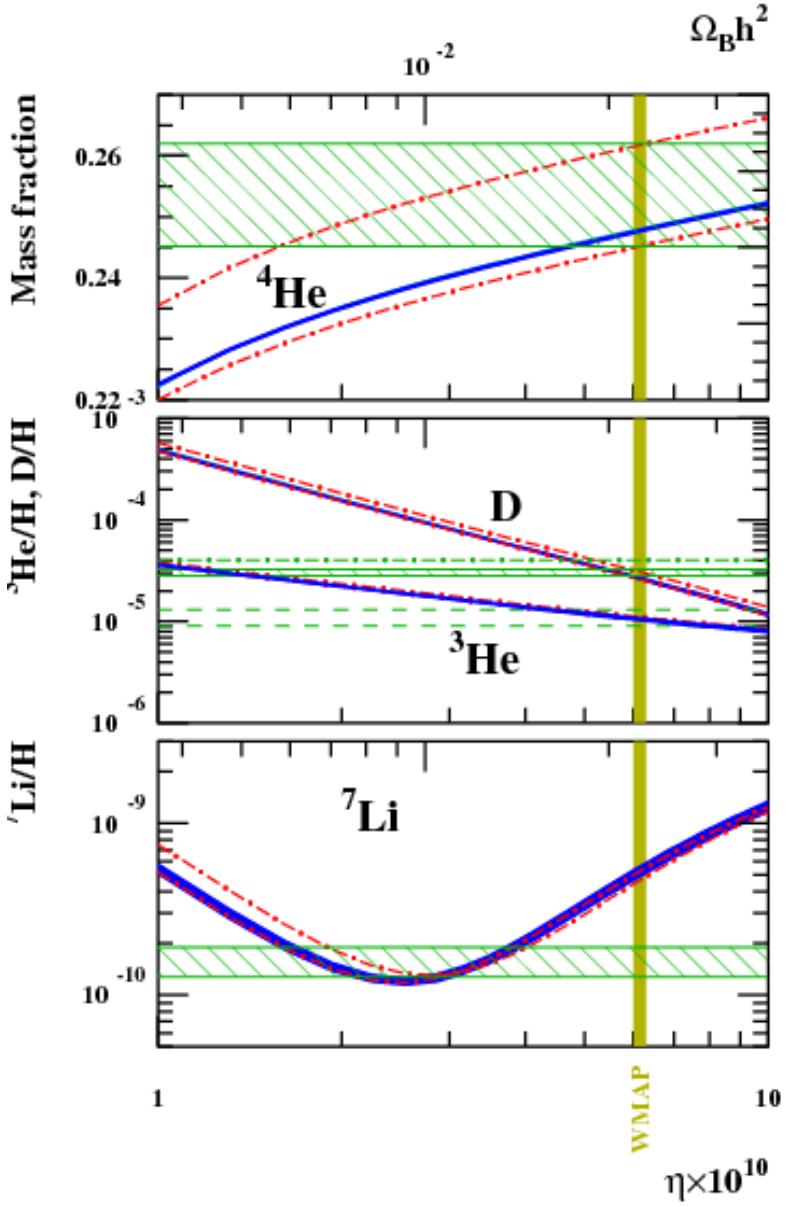

Quant.	Dominant Theoretical Error Sources in %							
Φ(pp)	$L_\odot$:	0.3	S_{34}:	0.3	κ:	0.2	Diff:	0.2
Φ(pep)	κ:	0.5	$L_\odot$:	0.4	S_{34}:	0.4	S_{11}:	0.2
Φ(hep)	S_{hep}:	30.2	S_{33}:	2.4	κ:	1.1	Diff:	0.5
Φ(^{7}Be)	S_{34}:	4.1	κ:	3.8	S_{33}:	2.3	Diff:	1.9
Φ(^{8}B)	κ:	7.3	S_{17}:	4.8	Diff:	4.0	S_{34}:	3.9
Φ(^{13}N)	C:	10.0	S_{114}:	5.4	Diff:	4.8	κ:	3.9
Φ(^{15}O)	C:	9.4	S_{114}:	7.9	Diff:	5.6	κ:	5.5
Φ(^{17}F)	O:	12.6	S_{116}:	8.8	κ:	6.0	Diff:	6.0

Vinyoles et al.,
The Astrophysical Journal,
835, 202 (2017)

Tamás Szücs | tszucs@atomki.hu | 27.02.2024

Reaction level scheme

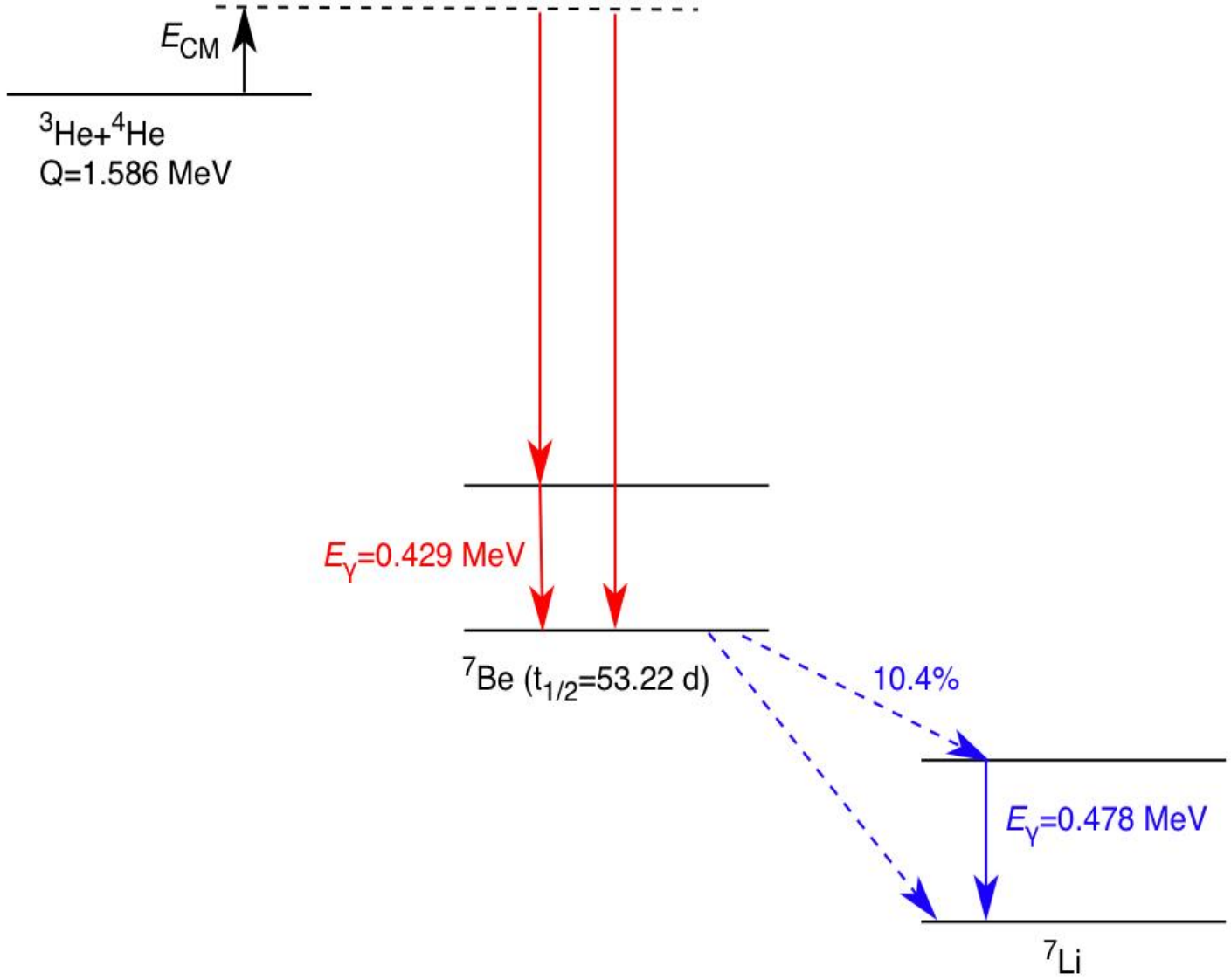

Tamás Szücs | tszucs@atomki.hu | 27.02.2024

Nuclear reaction cross section (σ) for charged particles

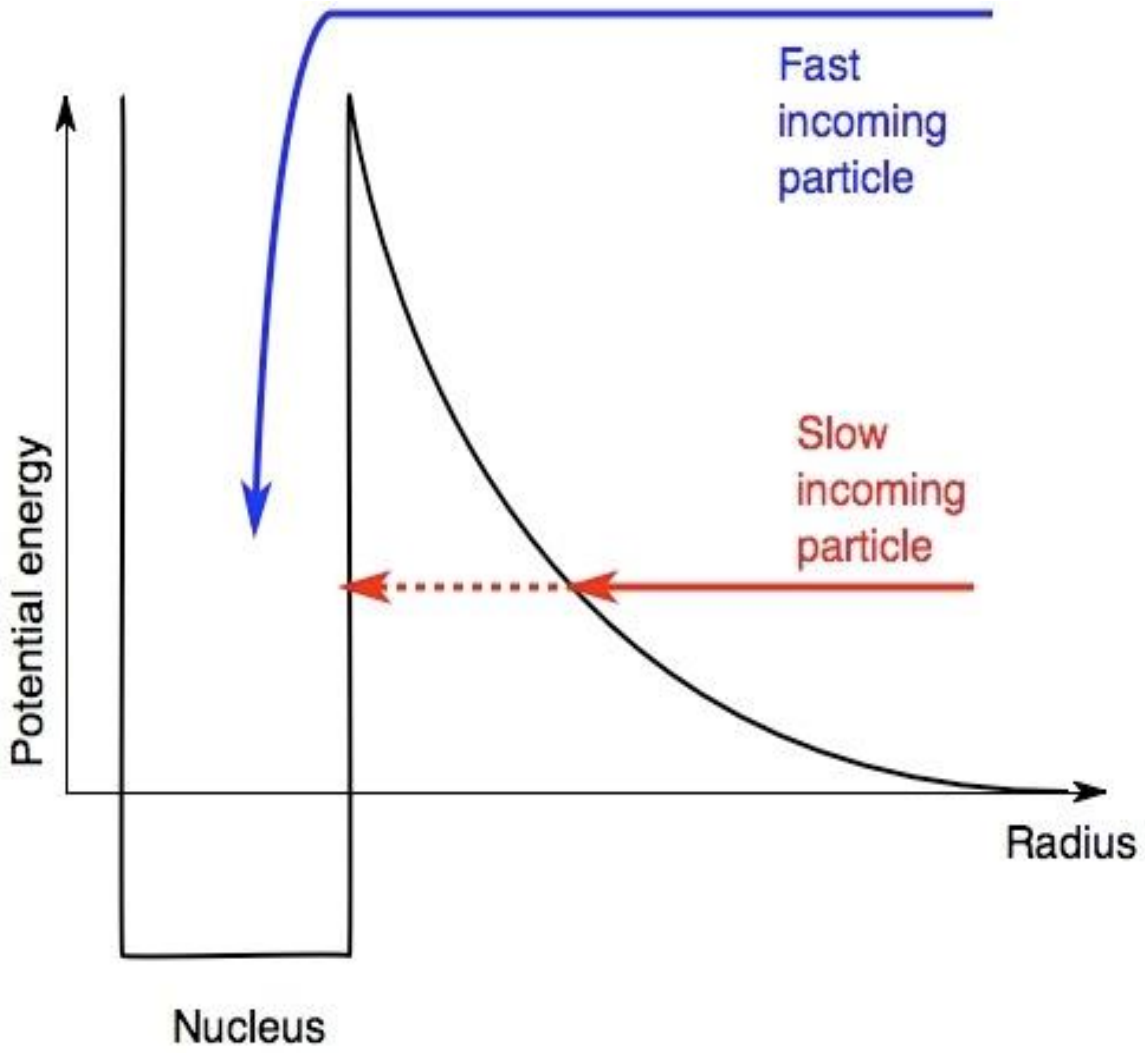

Typical Coulomb barrier height : ~ MeV

Typical temperature $k_B * T$ ~ keV

→The energy dependence of the cross section is dominated by the tunneling probability.

Tunneling probability
(for relative angular momentum l=0):

$$\propto \exp\left[-\alpha Z_1 Z_2 \sqrt{\frac{\mu}{E}}\right]$$

Tamás Szücs | tszucs@atomki.hu | 27.02.2024

Extrapolation and the astrophysical S-factor

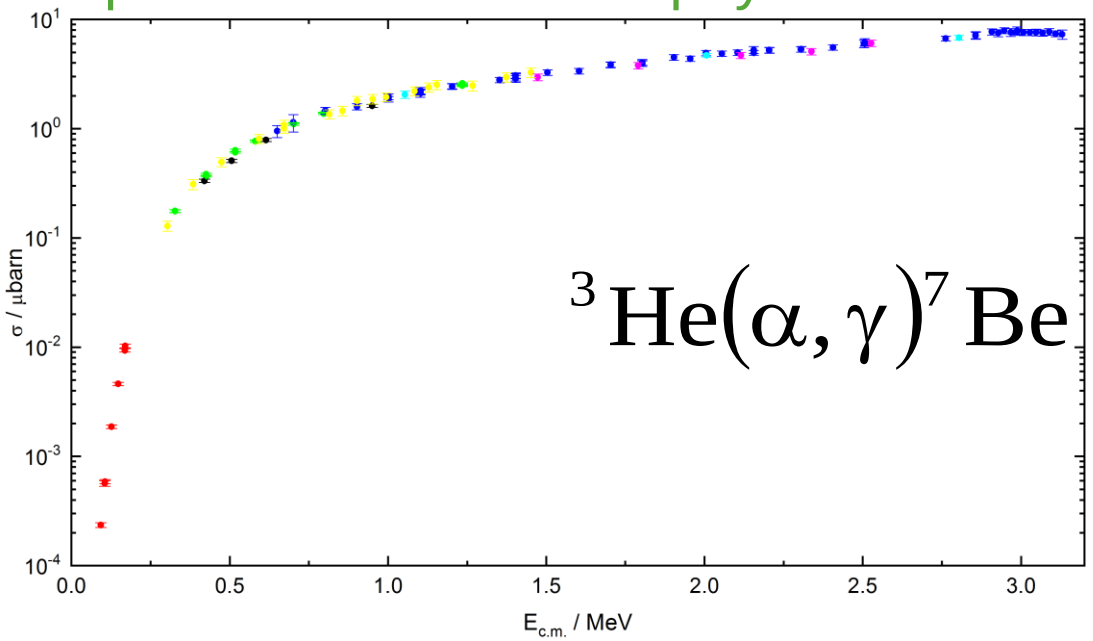

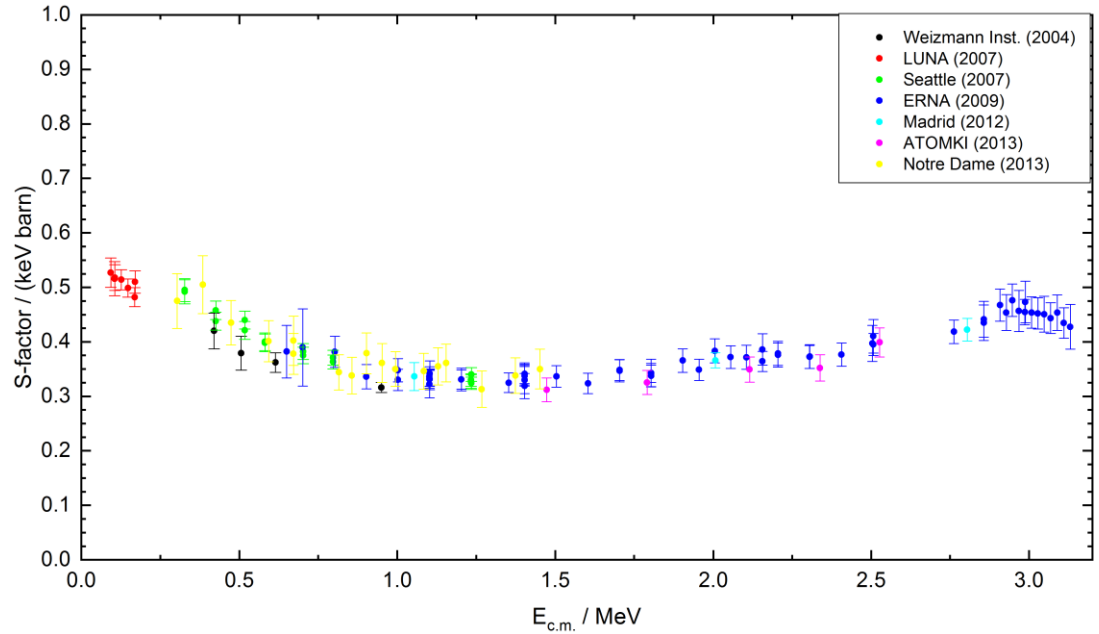

$$\sigma(E) \equiv \frac{1}{E} e^{-2\pi\eta} S(E)$$

Geometrical cross section

s-wave Coulomb Barrier transmission

Scenario	E_G [keV]	σ [barn]	Detected events/ hour
Sun (16 MK)	23	10^{-17}	10^{-9}
Big bang (300 MK)	160	10^{-9}	10^{-1}

Tamás Szücs | tszucs@atomki.hu | 27.02.2024

SFI and SFII (Solar fusion cross sections)

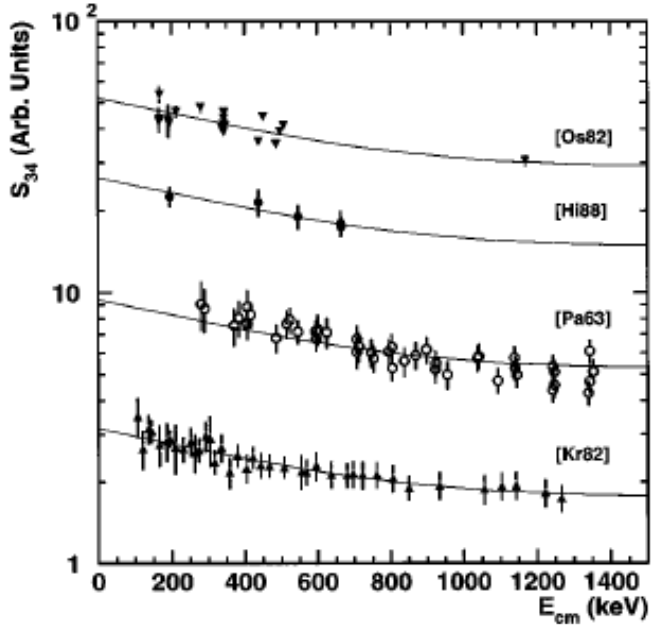

TABLE II. Measured values of $S_{34}(0)$.

$S_{34}(0)$ (keV b)	Reference
Measurement of capture γ rays:	
0.47±0.05	Parker and Kavanagh (1963)
0.58±0.07	Nagatani, Dwarakanath, and Ashery (1969)[a]
0.45±0.06	Kräwinkel *et al.* (1982)[b]
0.52±0.03	Osborne *et al.* (1982, 1984)
0.47±0.04	Alexander *et al.* (1984)
0.53±0.03	Hilgemeier *et al.* (1988)
Weighted Mean=0.507±0.016	
Measurement of ^{7}Be activity:	
0.535±0.04	Osborne *et al.* (1982, 1984)
0.63±0.04	Robertson *et al.* (1983)
0.56±0.03	Volk *et al.* (1983)
Weighted Mean=0.572±0.026	

[a]As extrapolated using the direct-capture model of Tombrello and Parker (1963).
[b]As renormalized by Hilgemeier *et al.* (1988).

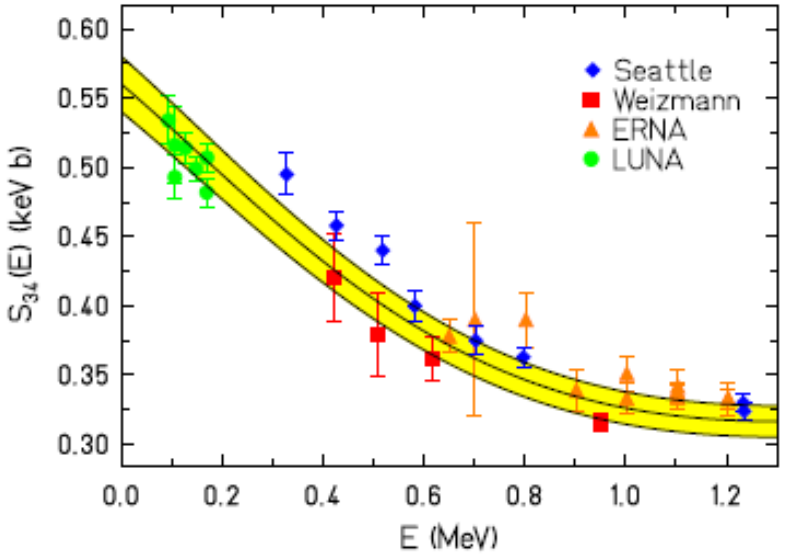

TABLE III. Experimental $S_{34}(0)$ values and 1-σ uncertainties determined from fits of the scaled Nollett (Kim A potential) theory to published data with $E \leq 1.002$ MeV. Total errors are quoted, including inflation factors, and systematic errors of LUNA: ±2.9%; Weizmann: ±2.2%; UW–Seattle: ±3.0%; ERNA: ±5.0%.

Experiment	$S_{34}(0)$ (keV b)	Error (keV b)	Inflation Factor
LUNA	0.550	0.017	1.06
Weizmann	0.538	0.015	1.00
UW–Seattle	0.598	0.019	1.15
ERNA	0.582	0.029	1.03
Combined result	0.560	0.016	1.72

SFI: Adelberger *et al.*, Rev. Mod. Phys. **70**, 1265 (1998) SFII: Adelberger *et al.*, Rev. Mod. Phys. **83**, 195 (2011)

Tamás Szücs | tszucs@atomki.hu | 27.02.2024

Post-2000 experimental data

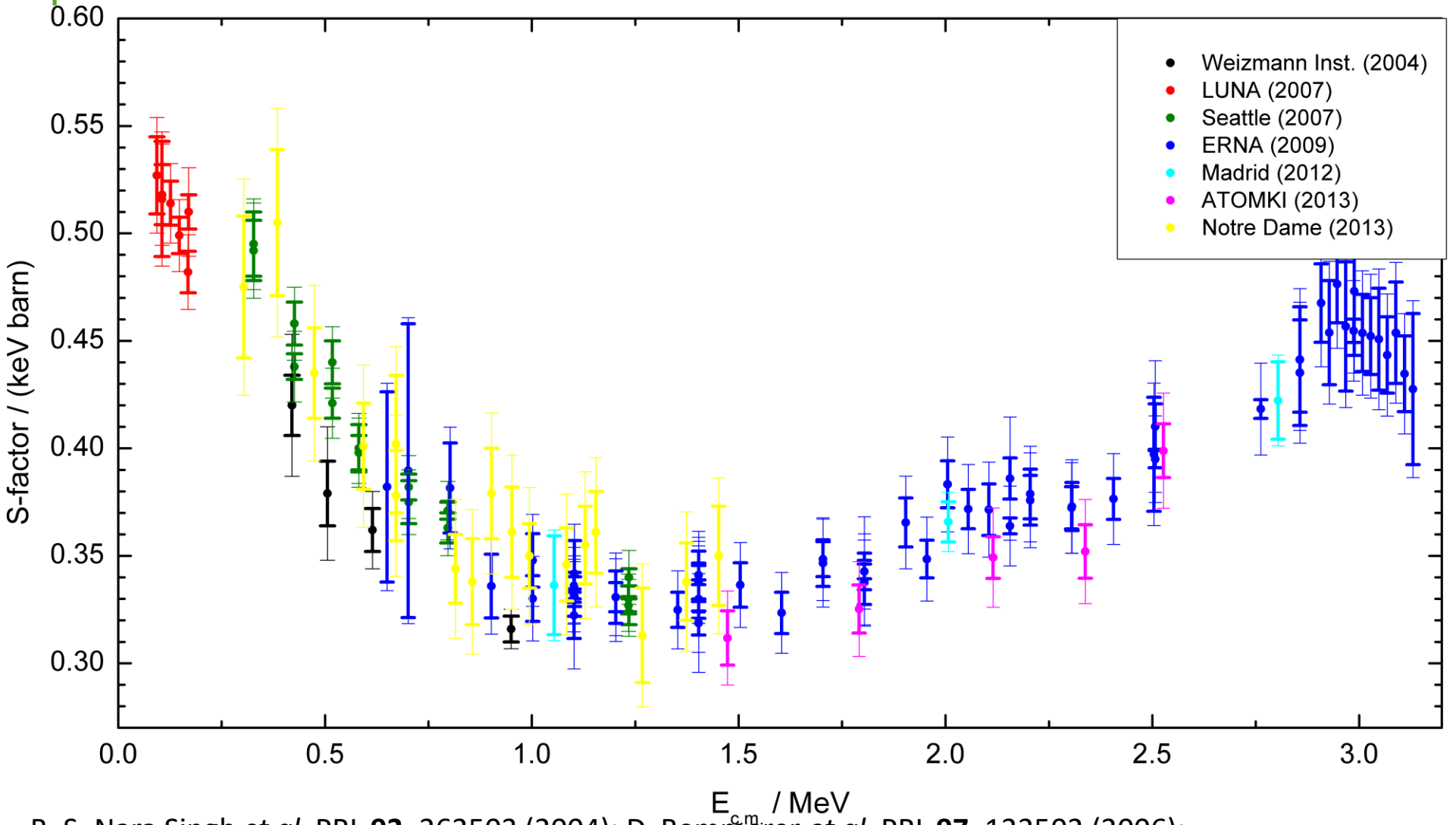

B. S. Nara Singh *et al*, PRL **93,** 262503 (2004); D. Bemmerer *et al*, PRL **97,** 122502 (2006);
T. A. D. Brown *et al*, PRC **76,** 055801 (2007); A. Di Leva *et al*, PRL **102,** 232502 (2009);
M. Carmona-Gallardo *et al*, PRC **86,** 032801(R) (2012);
C. Bordeanu *et al*, NPA **908,** 1 (2013); A. Kontos *et al*, PRC **87,** 065804 (2013)

Tamás Szücs | tszucs@atomki.hu | 27.02.2024

Microscopic calculations

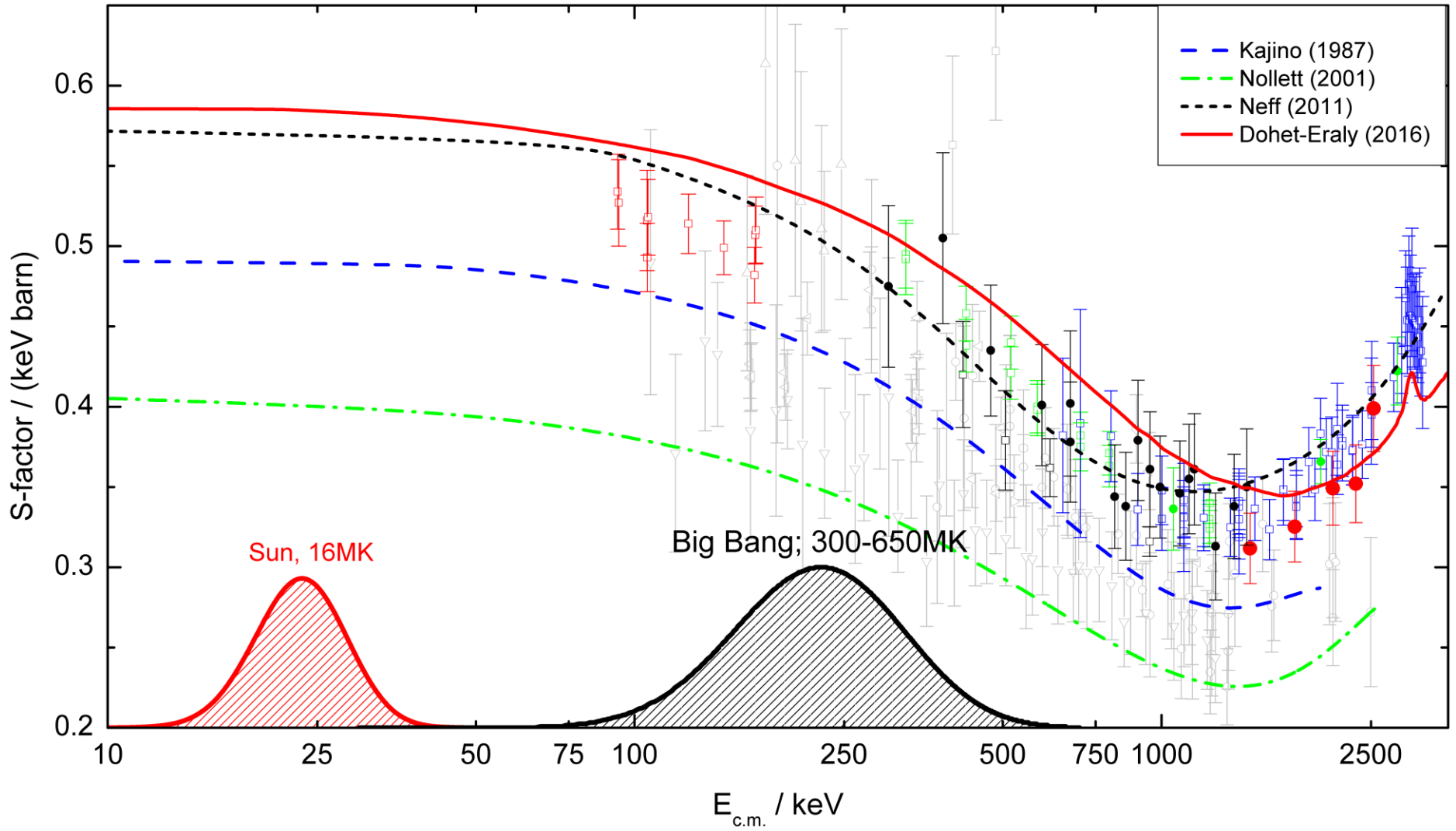

T. Kajino *et al*, ApJ **319,** 531 (1987); K. M. Nollett, PRC **63,** 054002 (2001);
T. Neff, PRL **106,** 042502 (2011); J. Dohet-Eraly *et al*, PLB **757,** 430 (2016)

Levels of ^{7}Be

Levels known from scattering experiments

Proposed level, which was not confirmed

Capture datasets cover this energy range

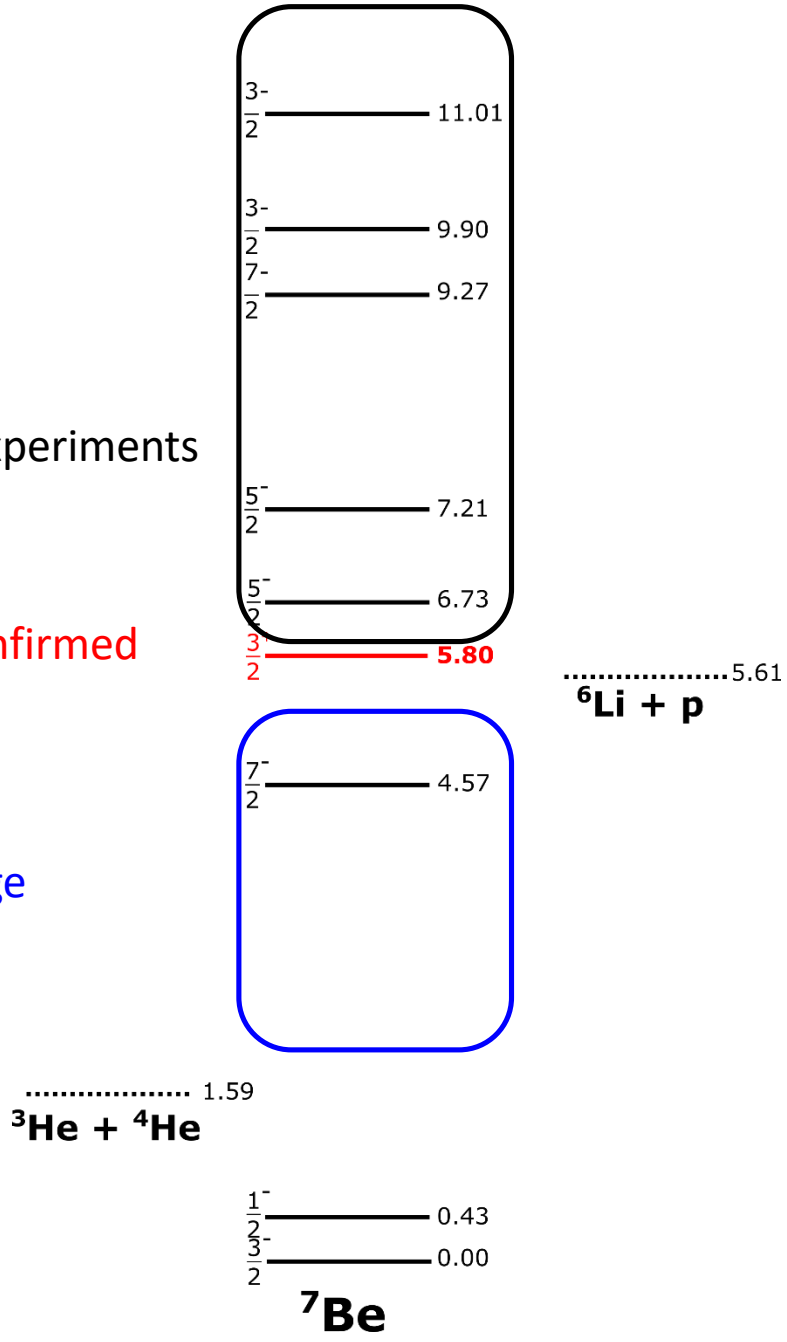

Tamás Szücs | tszucs@atomki.hu | 27.02.2024

$^{6}Li(p,\gamma)^{7}Be$ and the proposed positive parity level

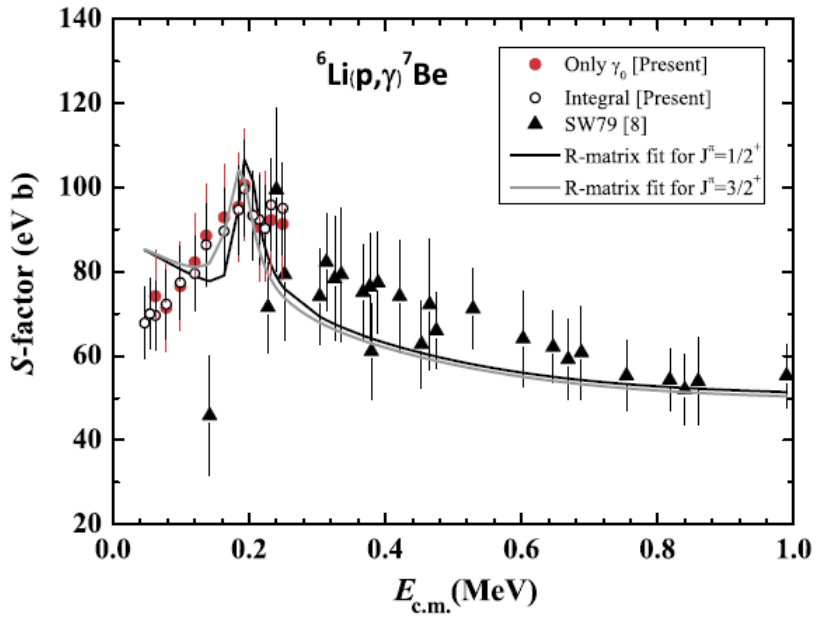

J. J. He *et al*, PLB **725,** 287 (2013)

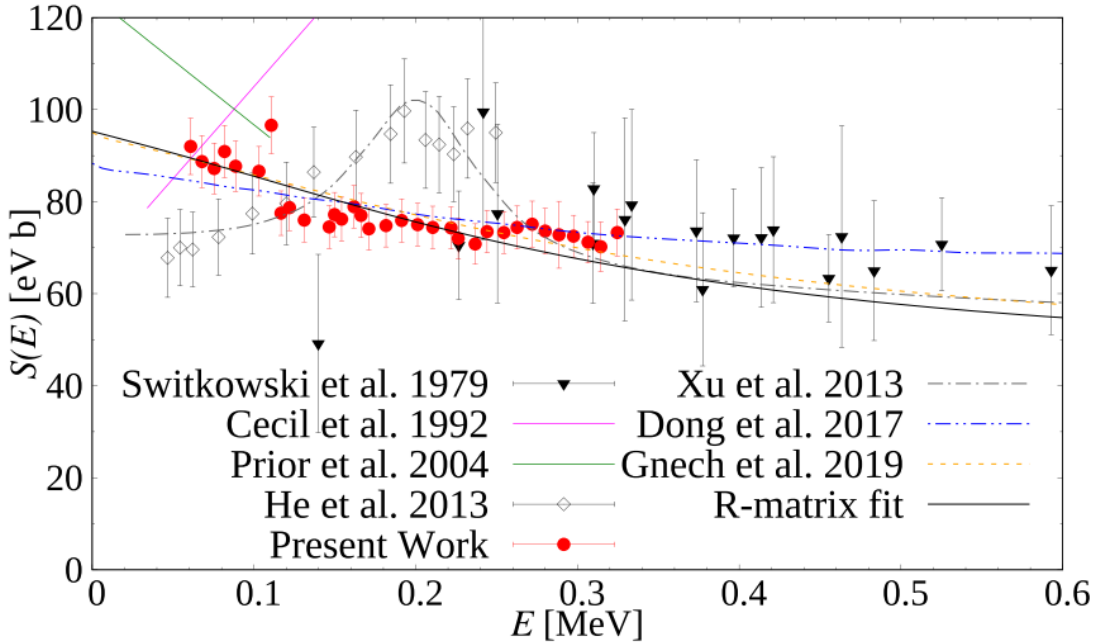

D. Piatti *et al*, PRC **102,** 052802(R) (2020)

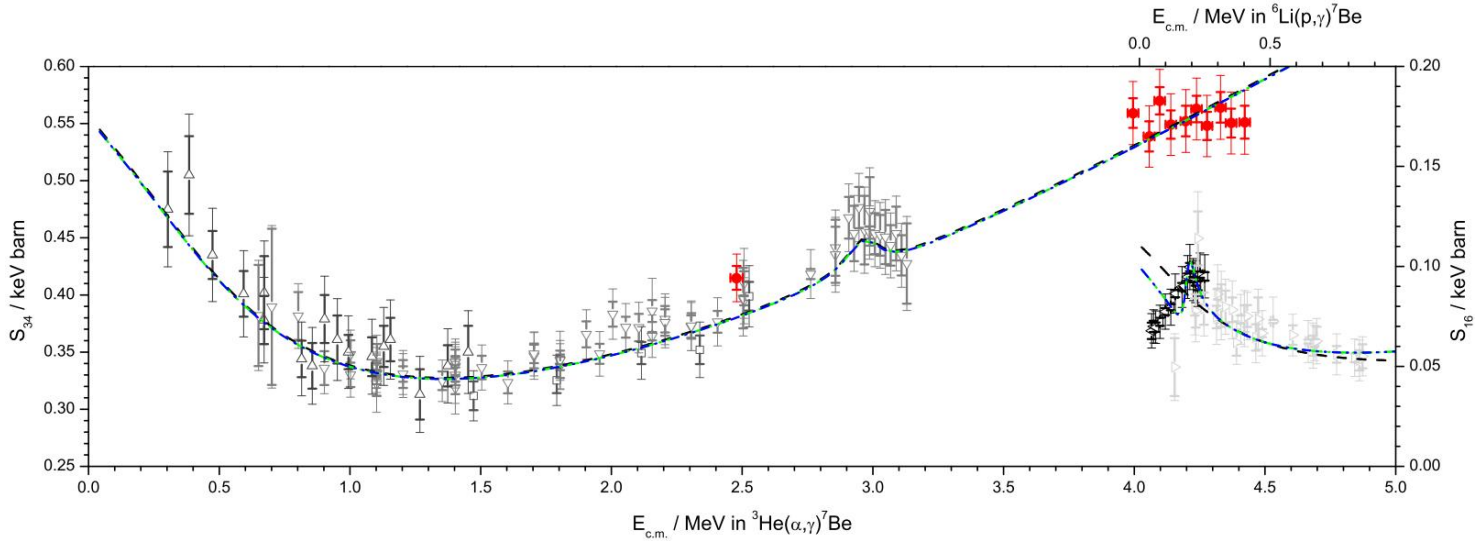

T. Szücs *et al*, PRC **99,** 055804 (2019)

Tamás Szücs | tszucs@atomki.hu | 27.02.2024

Thin window gas cell

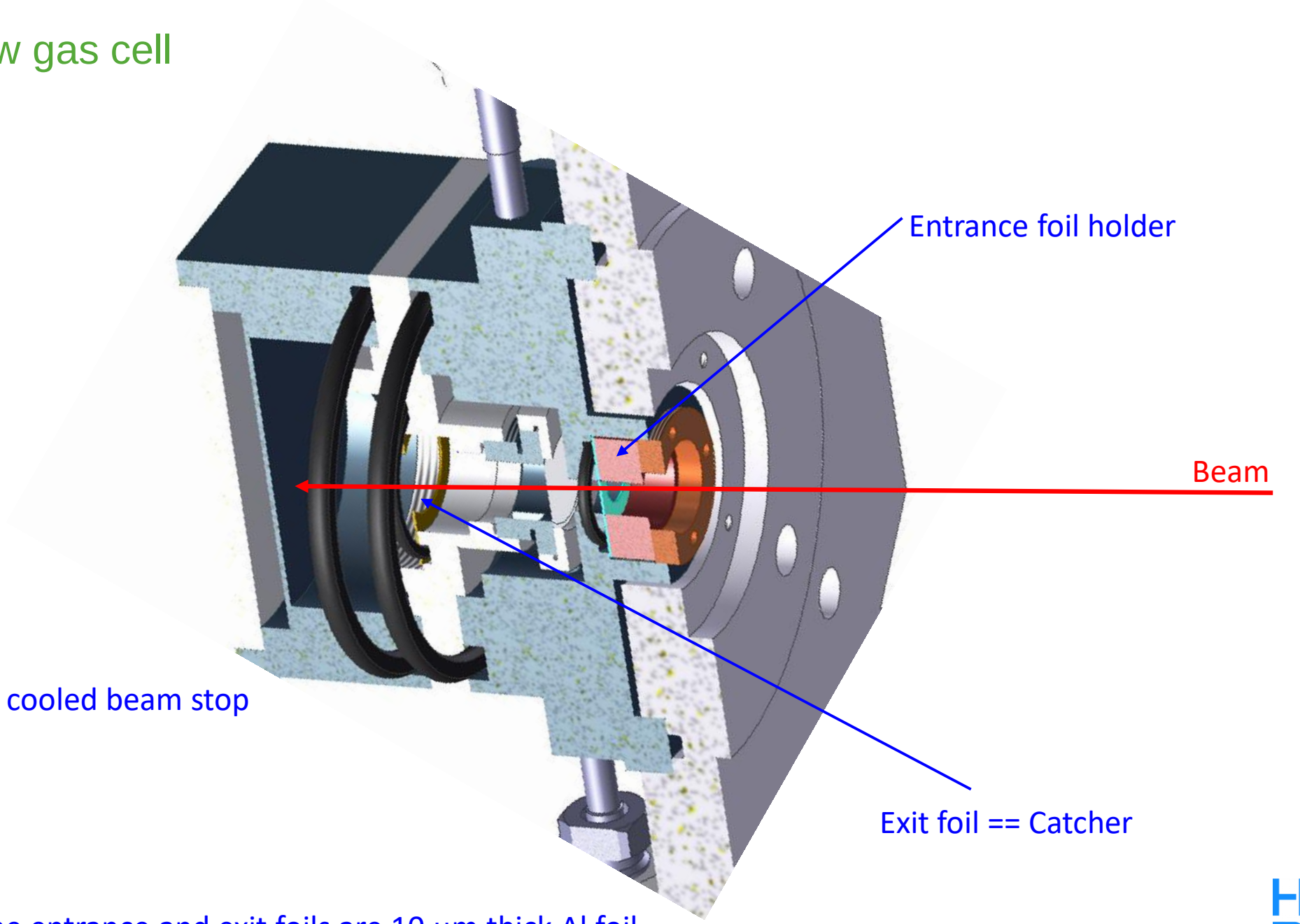

Both the entrance and exit foils are 10 μm thick Al foil

Tamás Szücs | tszucs@atomki.hu | 27.02.2024

Recoil separator

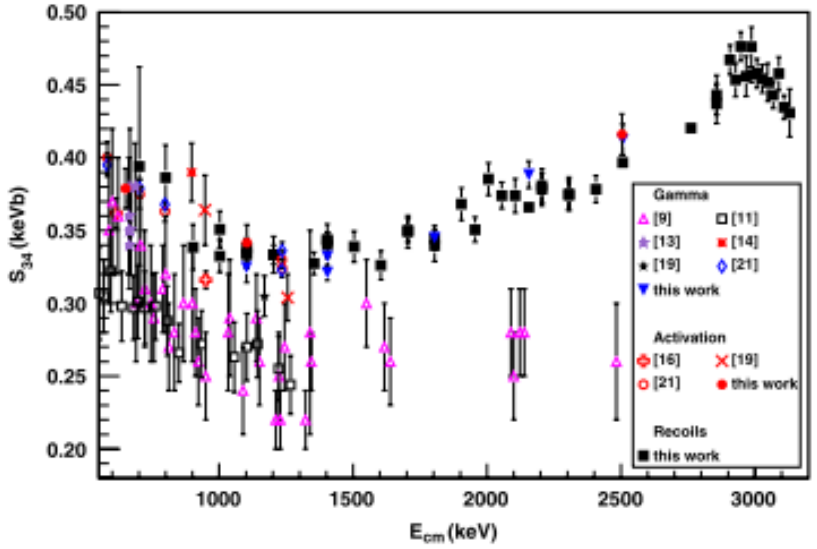

FIG. 1 (color online). Results of the cross section measurements of the present work. The data are plotted in the form of the astrophysical S factor as a function of the center-of-mass effective interaction energy. The results of previous work in the same energy range are also shown.

A. Di Leva et al, PRL **102**, 232502 (2009)

D. Schürmann et al, NIMA **531**, 428 (2004)

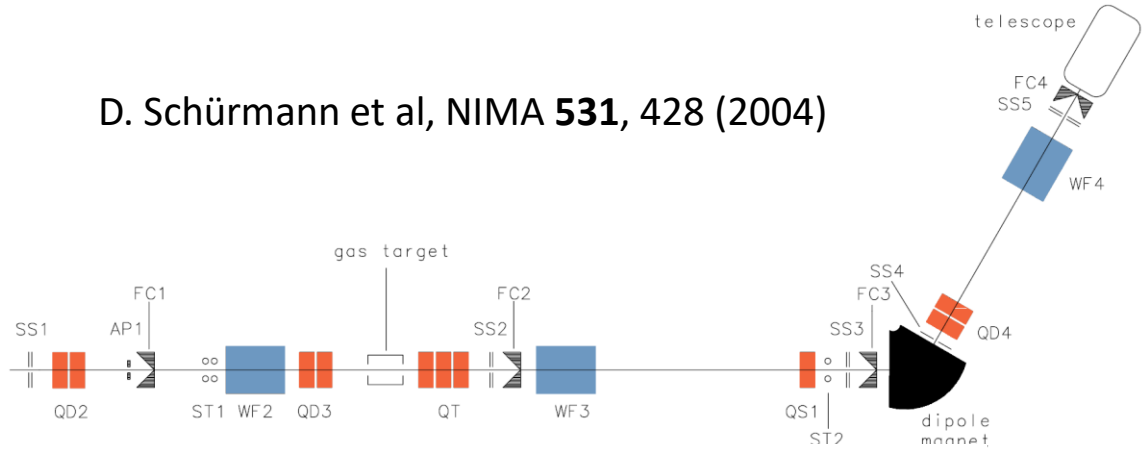

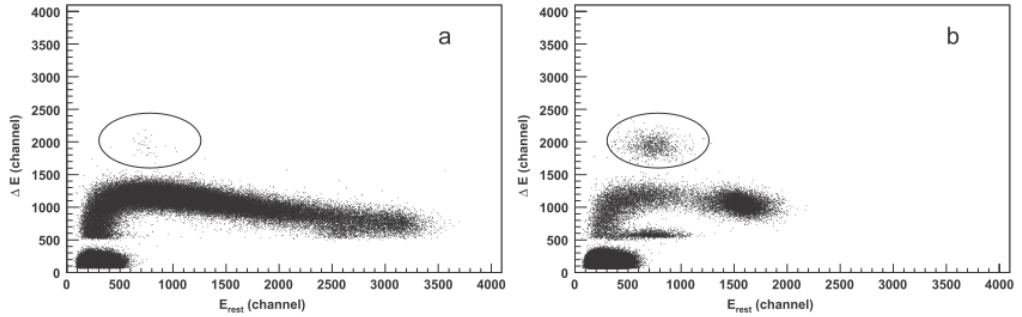

Fig. 10. $\Delta E-E$ matrices collected at $E_{cm} = 1.35$ MeV for the recoil charge state $q_{^7Be} = 1+$ (a) and $q_{^7Be} = 3+$ (b). The beam suppression factors of the separator are 1×10^{-11} and 1×10^{-12}, respectively. The regions where the ^{7}Be recoils are expected are indicated.

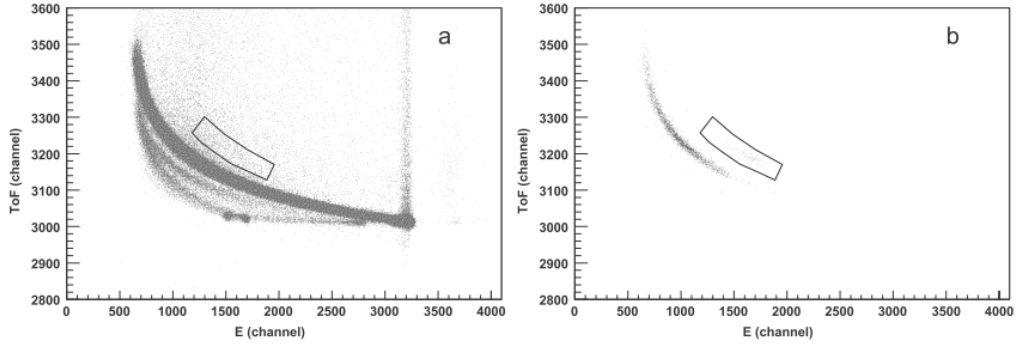

Fig. 11. TOF-E matrix collected at $E_{cm} = 0.8$ MeV for the recoil charge state $q_{^7Be} = 1+$ (a) and $q_{^7Be} = 3+$ (b). The beam suppression factors of the separator are 1×10^{-10} and 1×10^{-12}, respectively. The regions where the ^{7}Be recoils are expected are indicated. The structure below the main "leaky" ^{4}He component in (a) is due to ions impinging in the gaps between the strips, where a significant fraction of the energy of the incident particle is lost in the thick contact covering the sensitive volume. Moreover, the signal shape is deformed and the time signal is shifted by an amount that depends on the signal height.

A. Di Leva et al, NIMA **595**, 381 (2008)

Windowless gas target

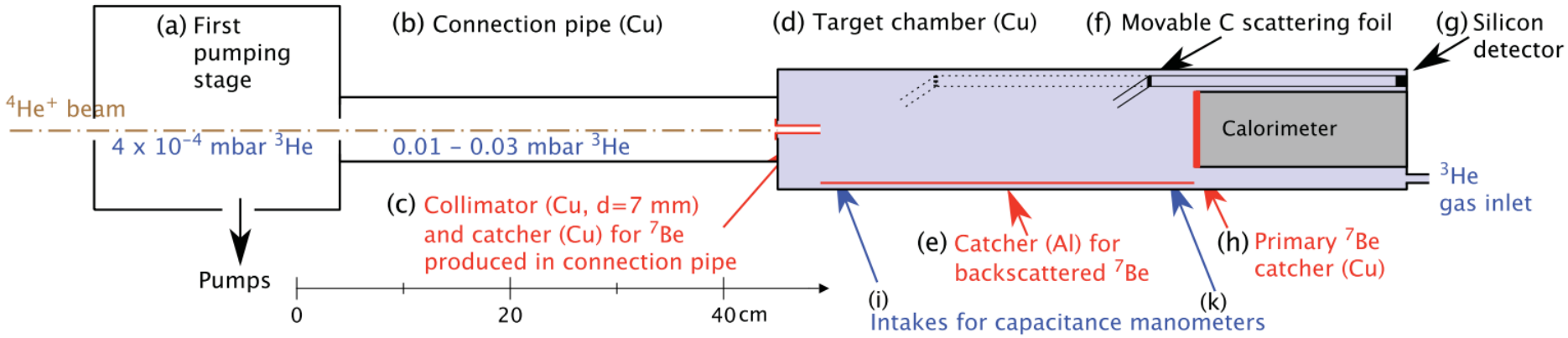

FIG. 2. (Color online) Schematic view of the target chamber used for the irradiations. See text for details.

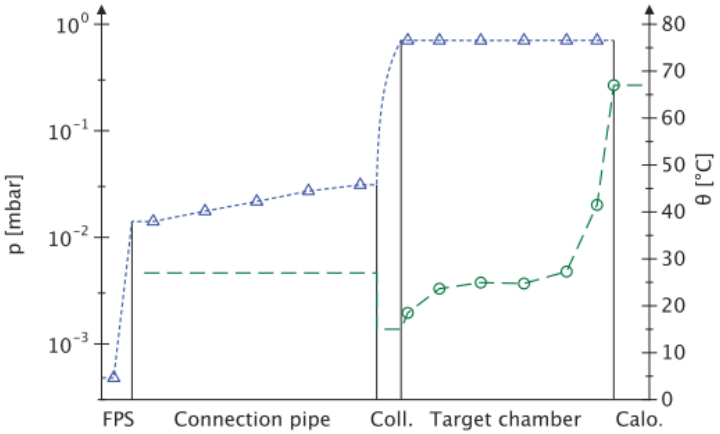

FIG. 3. (Color online) Measured pressure (p, blue triangles) and temperature (θ, green circles) profile inside the target chamber and adjacent regions: first pumping stage (FPS), connection pipe, collimator (Coll.), target chamber, and calorimeter (Calo.). The dashed lines indicate the interpolated profile adopted where there are no data.

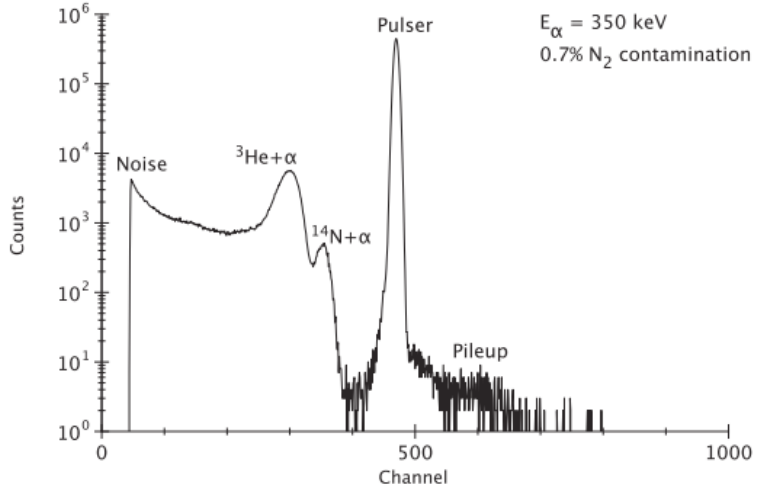

FIG. 4. Elastic scattering spectrum taken with the silicon detector at $E_\alpha = 350$ keV, showing a contamination of 0.7% N_2 in the ^{3}He gas.

D. Bemmerer et al (LUNA Collaboration), PRL **97**, 122502 (2006)
Gy. Gyürky et al (LUNA Collaboration), PRC **75**, 035805 (2007)

Windowless gas target

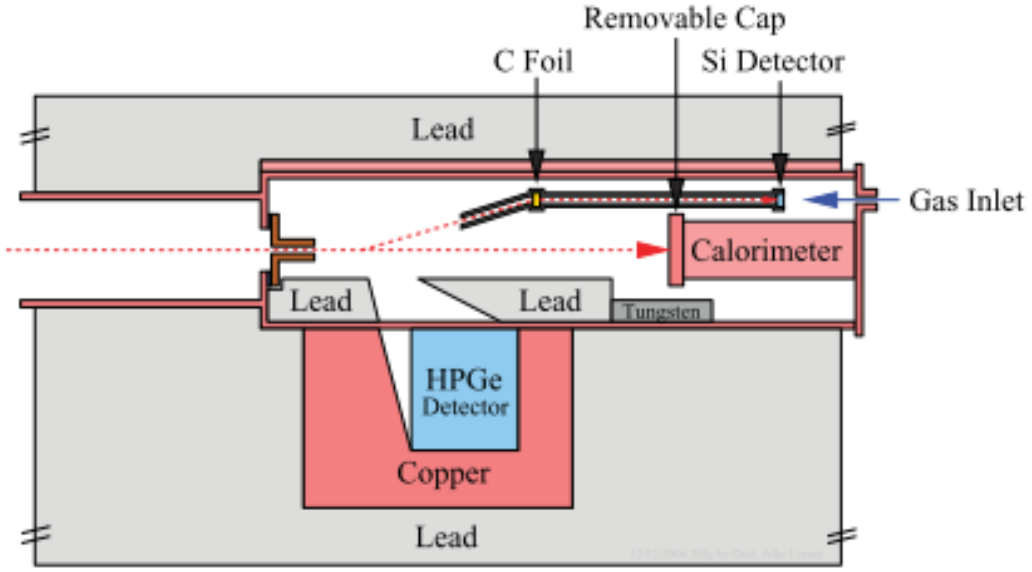

FIG. 1. (Color online) Schematic view of the interaction chamber with the position of the HPGe detector and of the 100 μm silicon detector used for ^{3}He density monitoring. The distance between the entrance collimator and the calorimeter is 35 cm. The thickness of the internal collimator is 3 cm for the Lead part and 1.6 cm for the tungsten part.

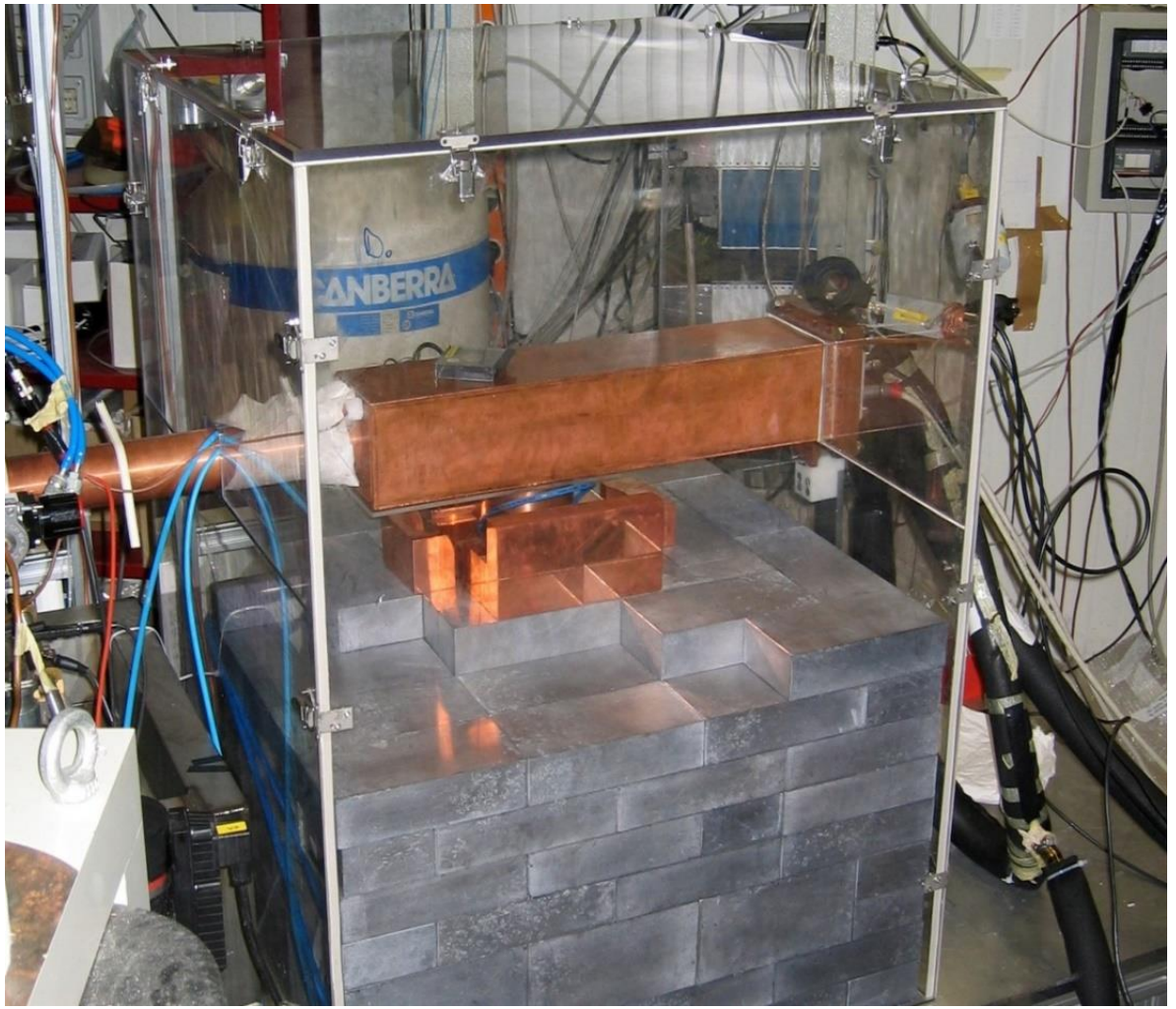

F. Confortola et al (LUNA Collaboration), PRC **75**, 065803 (2007)

Tamás Szücs | tszucs@atomki.hu | 27.02.2024

recent R-matrix fit

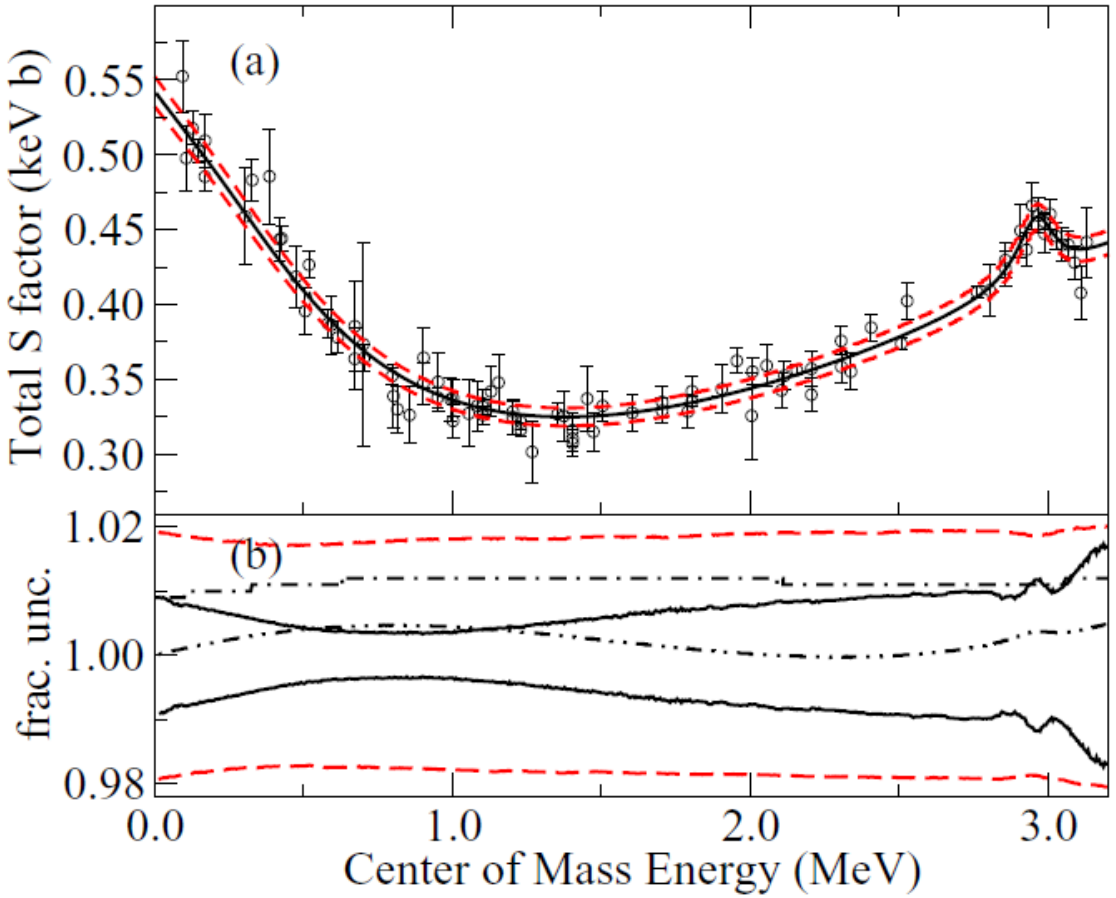

R. J. deBoer *et al*, PRC **90,** 035804 (2014)

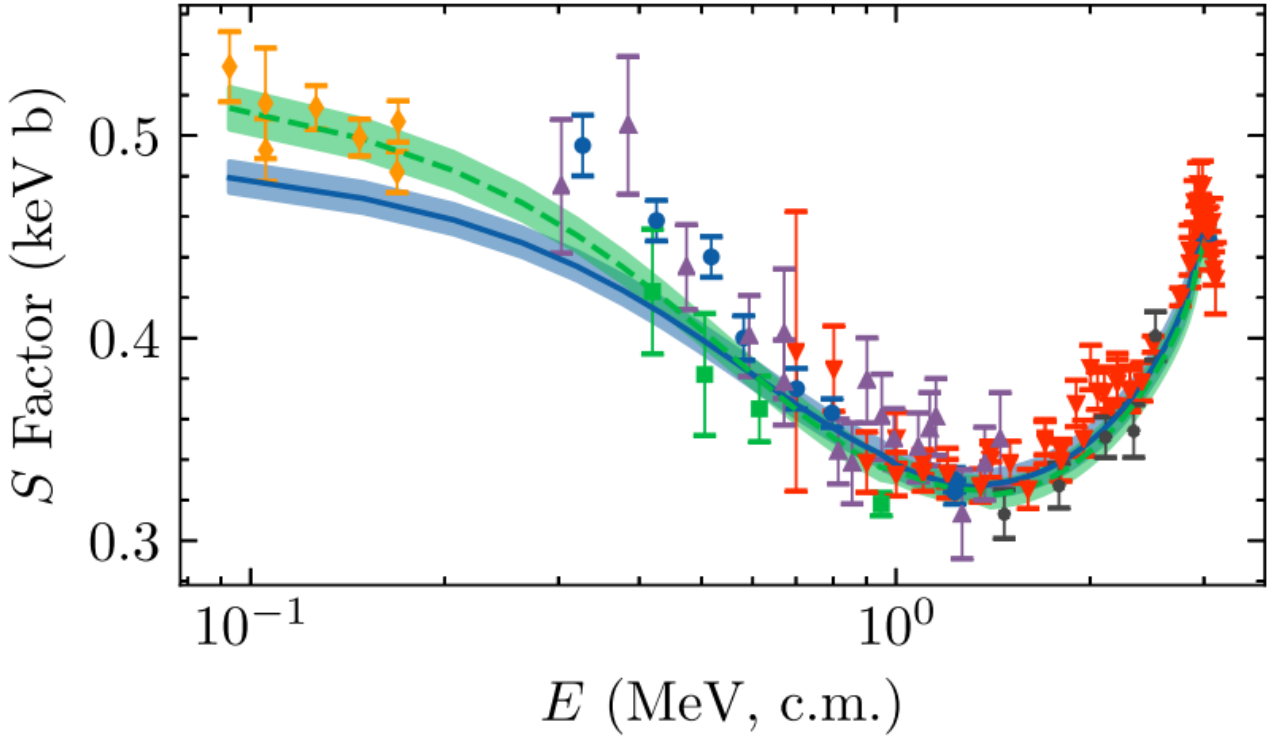

D. Odell *et al*, Frontiers **10**, 888476 (2022)

3He+4He elastic scattering

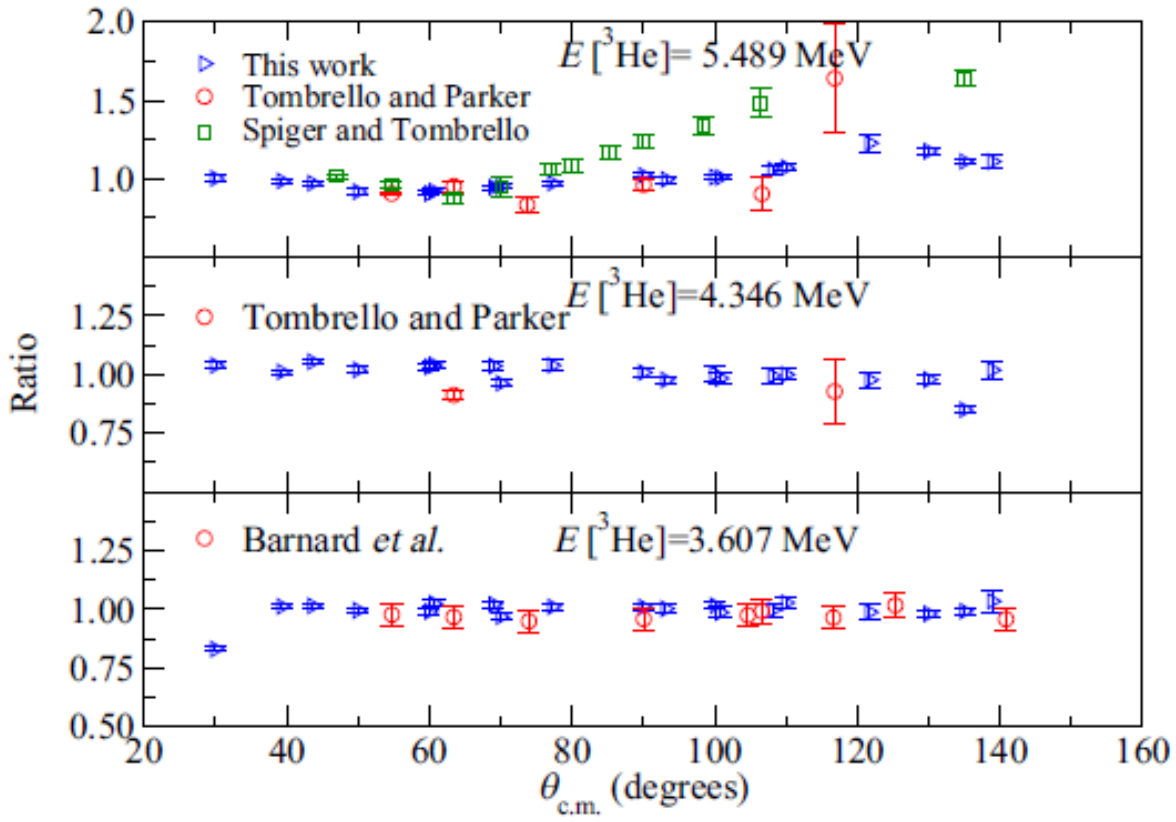

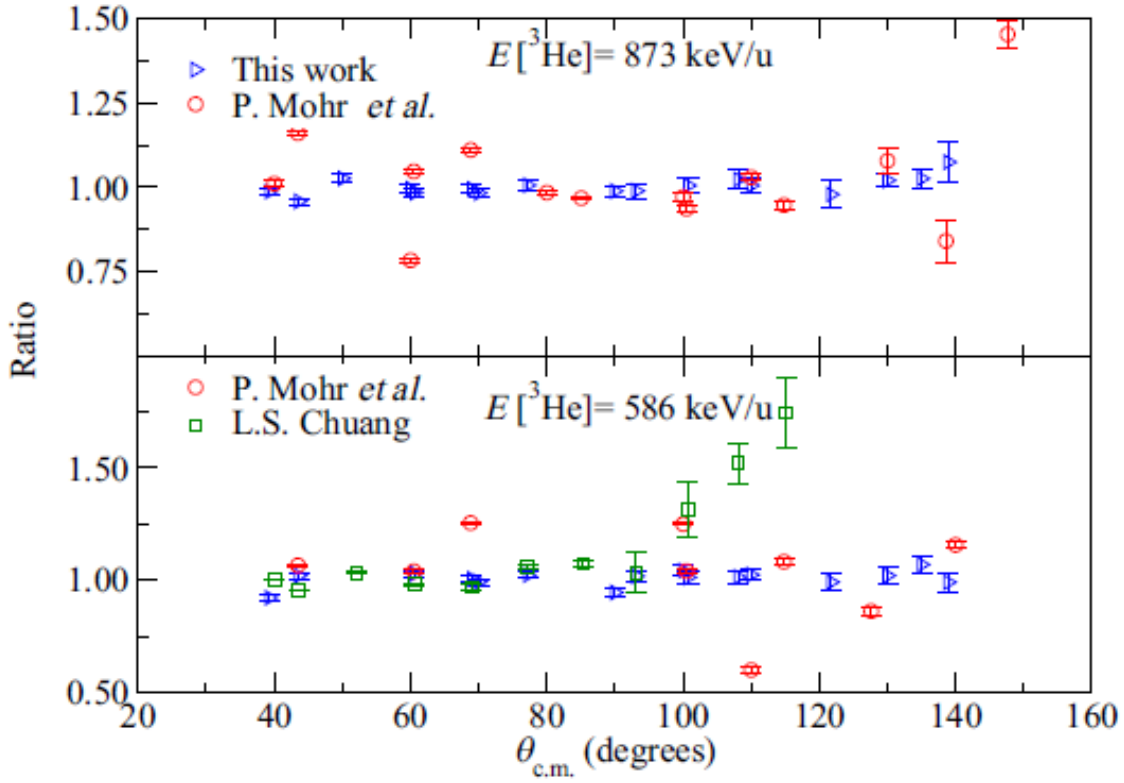

S. N. Paneru *et al*, PRC **109,** 015802 (2024)

ANCs from indirect technique

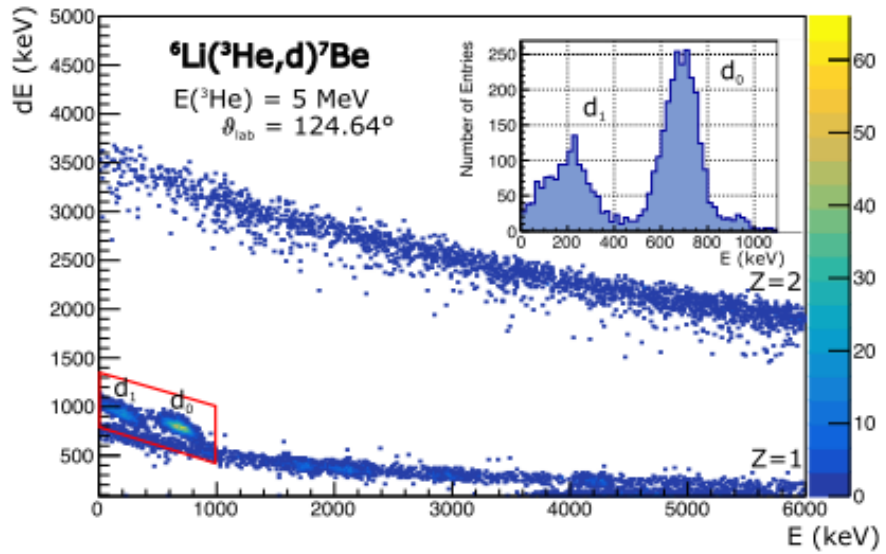

G. G. Kiss *et al*, PLB **807,** 135606 (2020)

The weighed mean values of the square of the ANCs for the $^3\mathrm{He} + \alpha \rightarrow {}^7\mathrm{Be}$(g.s.) and $^3\mathrm{He} + \alpha \rightarrow {}^7\mathrm{Be}$(0.429 MeV) are equal to C^2= 20.84 ± 1.12 [0.82; 0.77] fm^{-1} and C^2= 12.86 ± 0.50 [0.35; 0.36] fm^{-1}, respectively, which are in an excellent agree-

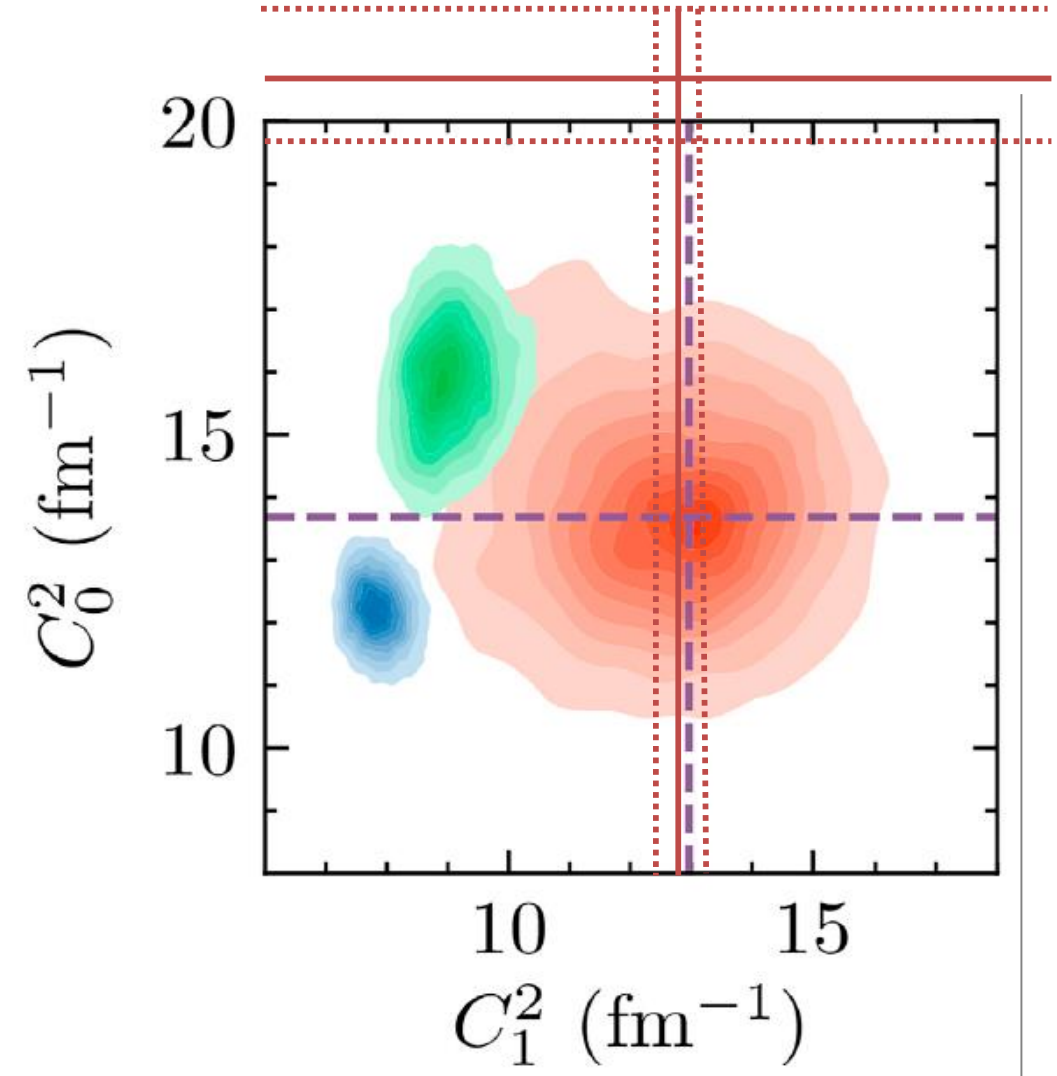

FIGURE 12 | The two-dimensional posterior of the squares of the ANCs, C_0 and C_1. Results for $\mathcal{D}_{CS}$ are shown in green and for $\mathcal{D}_{CSB}$ in blue. The EFT analysis of capture data of Zhang et al. [22] extracted the ANC values shown in red, and in the analysis of Barnard et al. [53] and capture data of deBoer et al. [7] the ANCs were fixed at the location indicated by the purple, dashed lines.

D. Odell *et al*, Frontiers **10**, 888476 (2022)

Other theoretical models (EFT: Effective Field Theory)

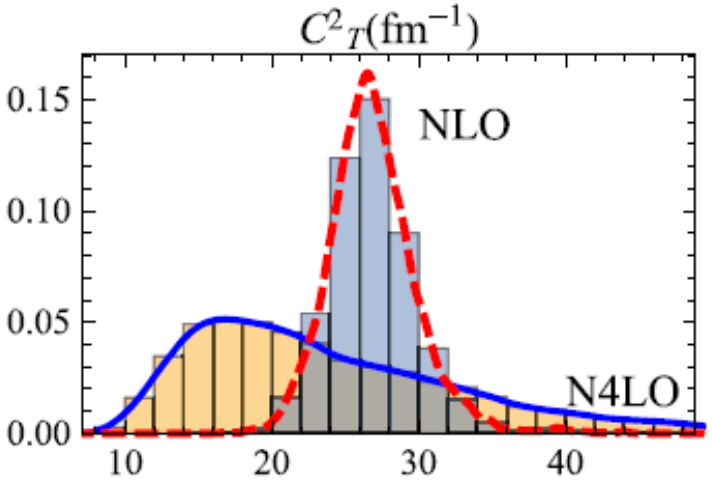

X. Zhang *et al*, J. Phys. G: Nucl. Part. Phys. **47,** 054002 (2020)

No-scattering constraint

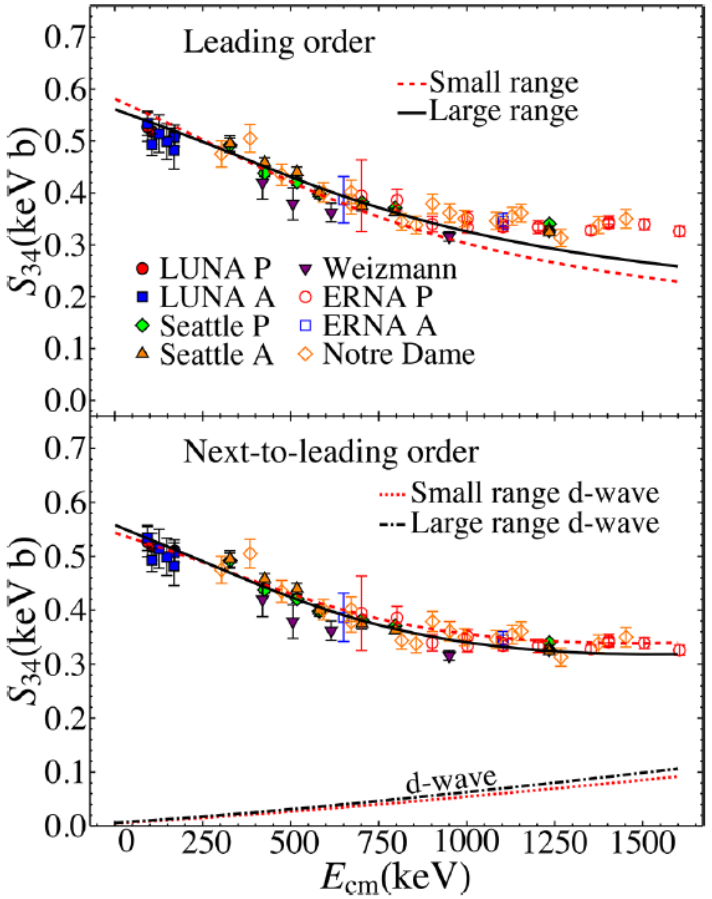

R. Higa, G. Rupak and A. Vaghani, Eur. Phys. J. A **54**, 89 (2018)

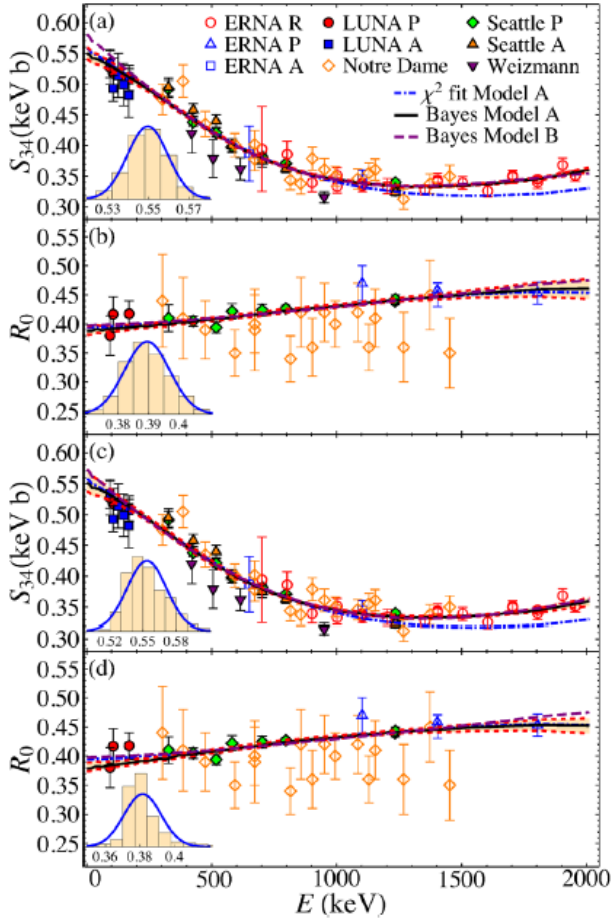

P. Premarathna and G. Rupak, Eur. Phys. J. A **56**, 166 (2020)

Scattering constraint from a phase shift analysis

Á. Tóth et al., PRC **108**, 025802 (2023)

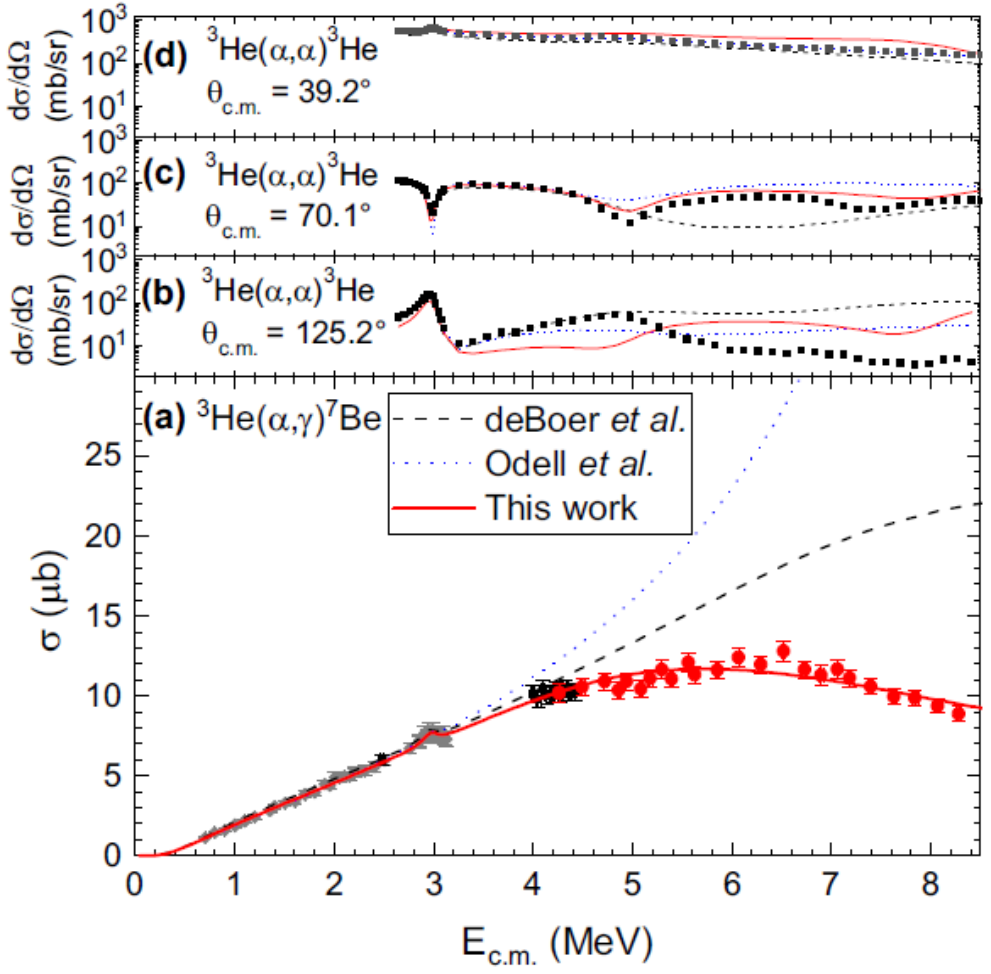

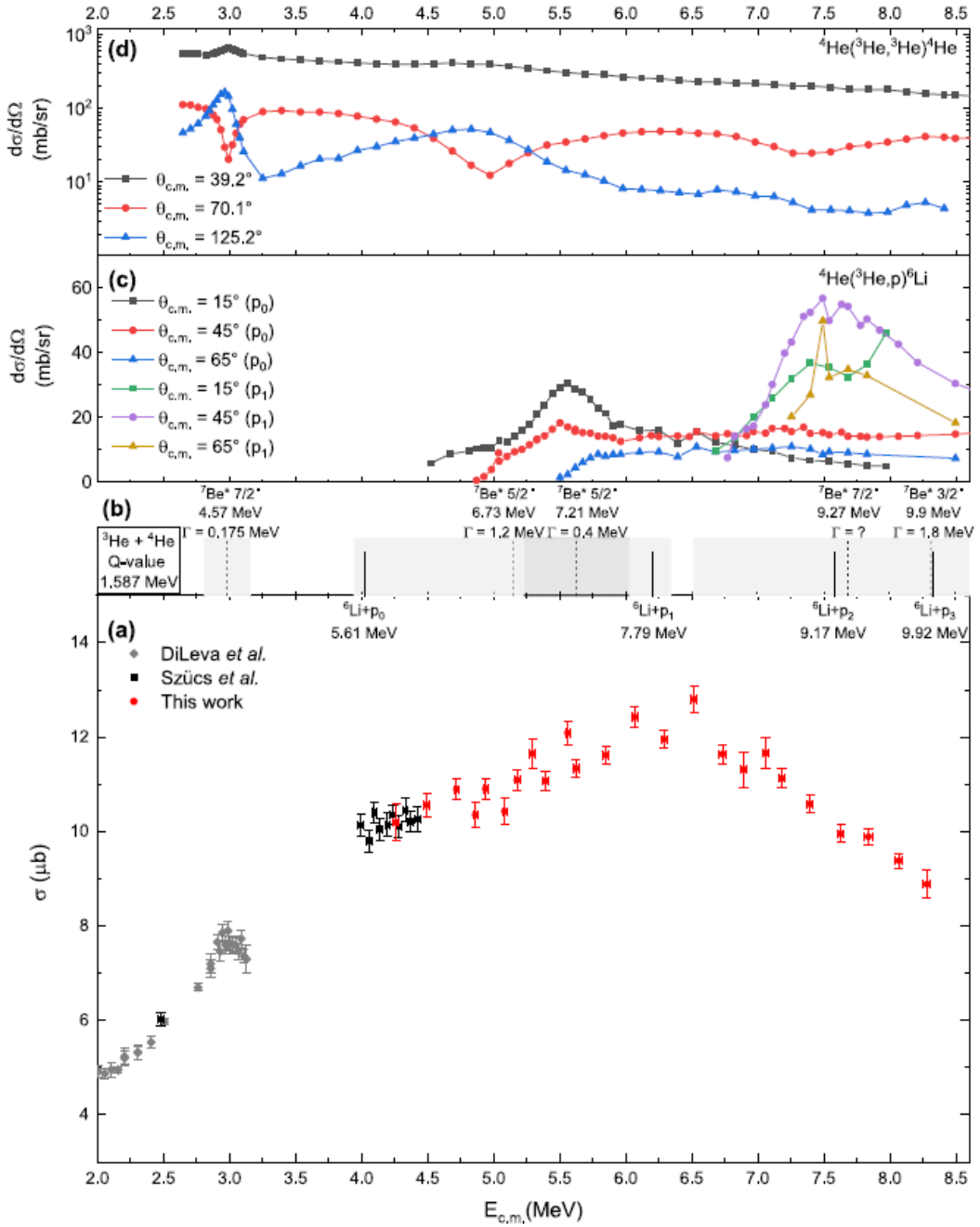

Experimental angular distribution of the prompt gamma-rays

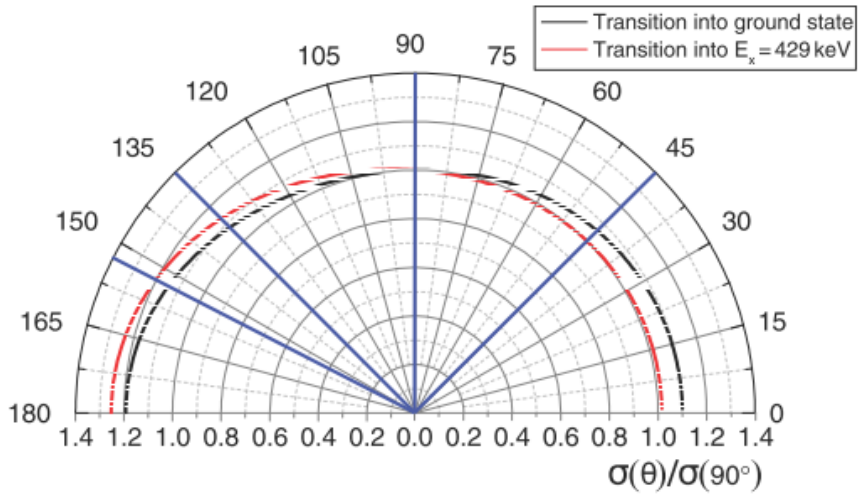

Figure 2. It is shown the predicted angular distribution for E = 2.9 MeV [2]. The position of the detectors during the measurement is indicated in blue.

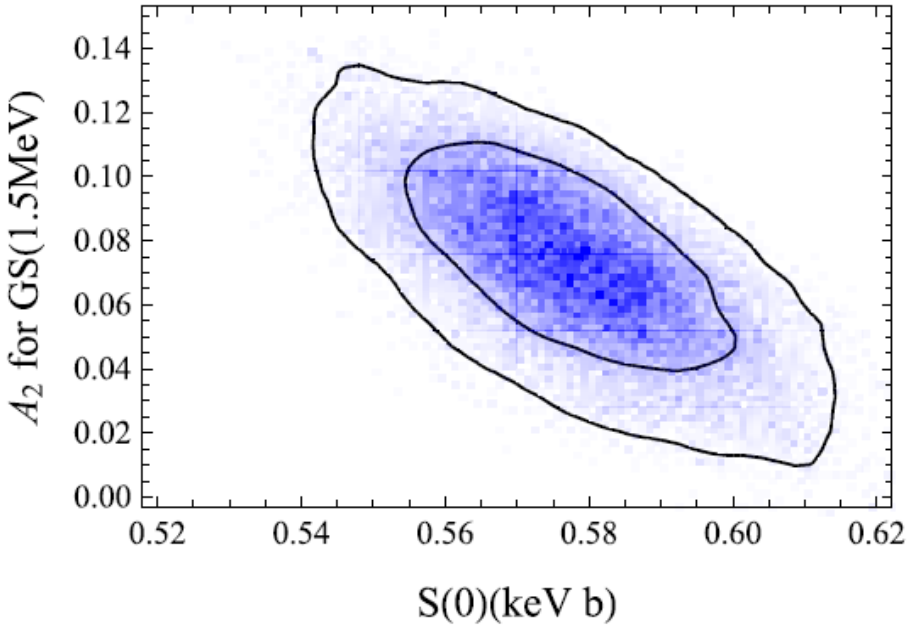

S. Turkat et al., Solar Neutrinos - Proceedings of the 5th International Solar Neutrino Conference, p 513 (2019)

S. Turkat, Ph.D. thesis, Technische Universität Dresden, 2023

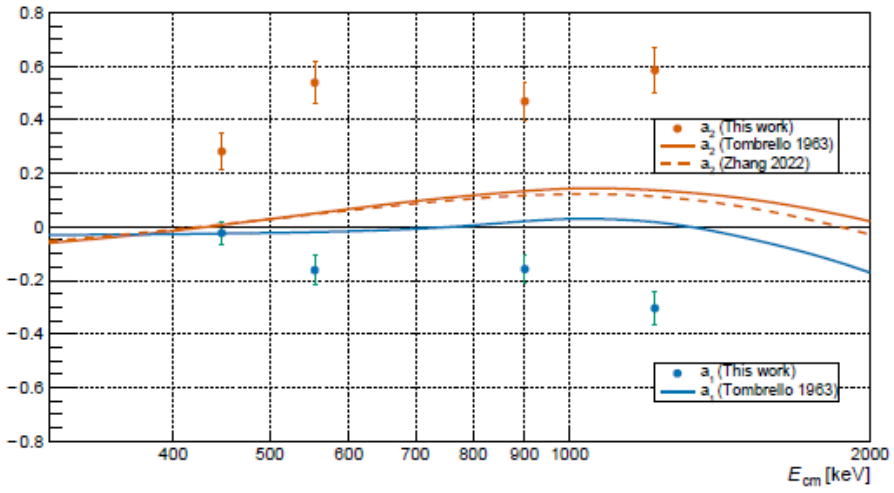

X. Zhang *et al*, J. Phys. G: Nucl. Part. Phys. **47,** 054002 (2020)

Experimental angular distribution of the prompt gamma-rays

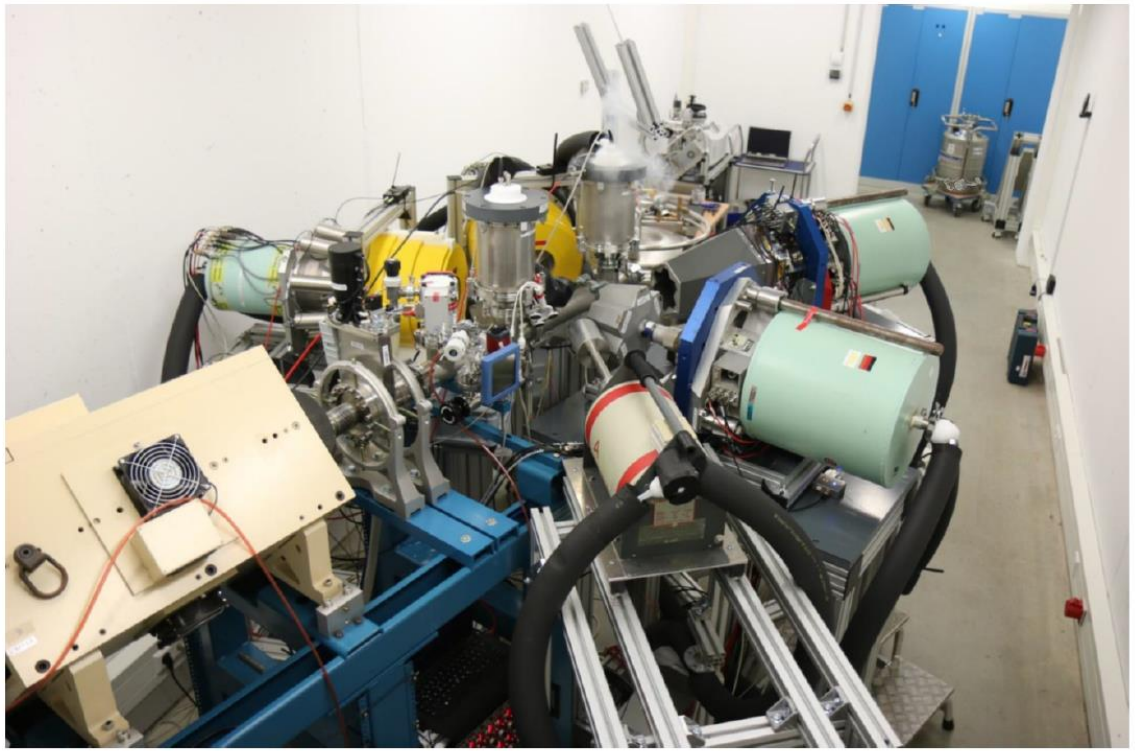

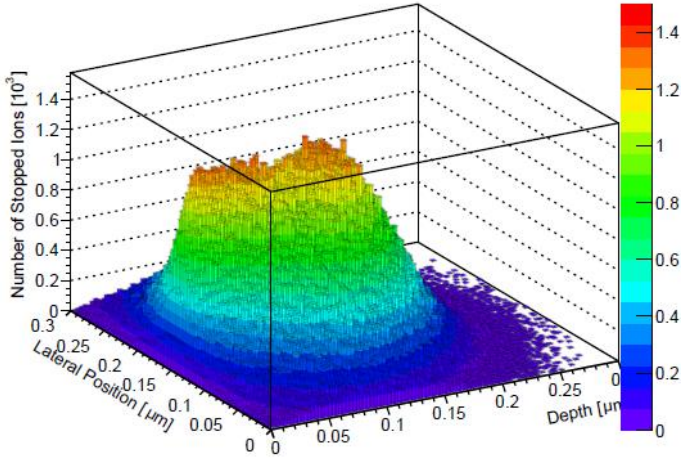

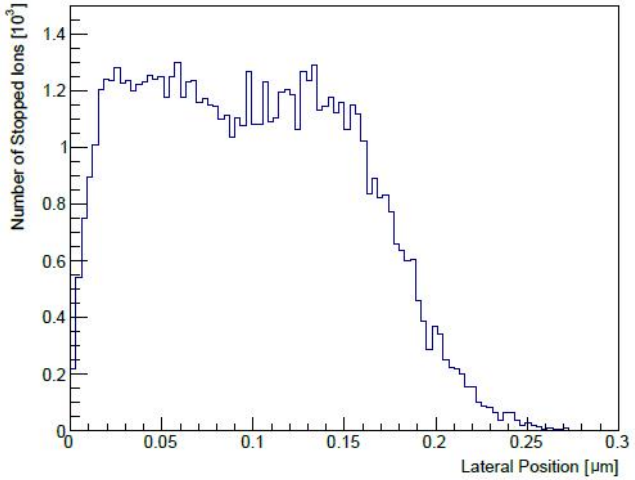

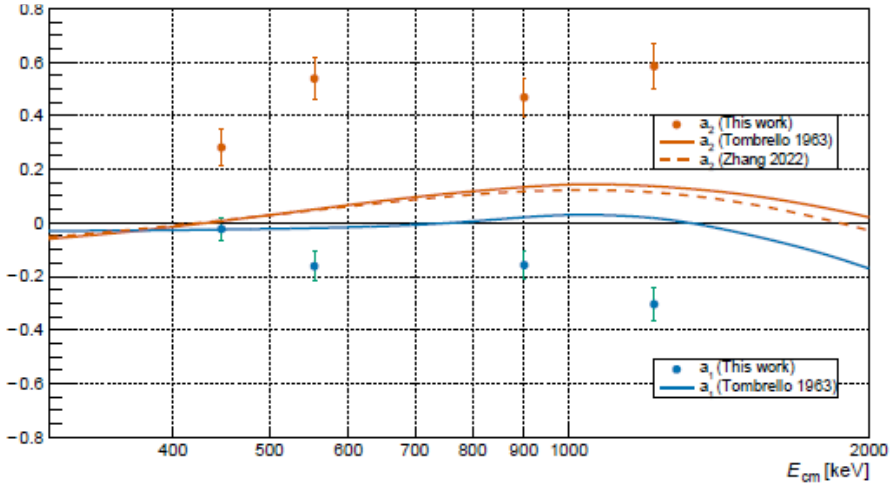

S. Turkat, Ph.D. thesis, Technische Universität Dresden, 2023

New target systems

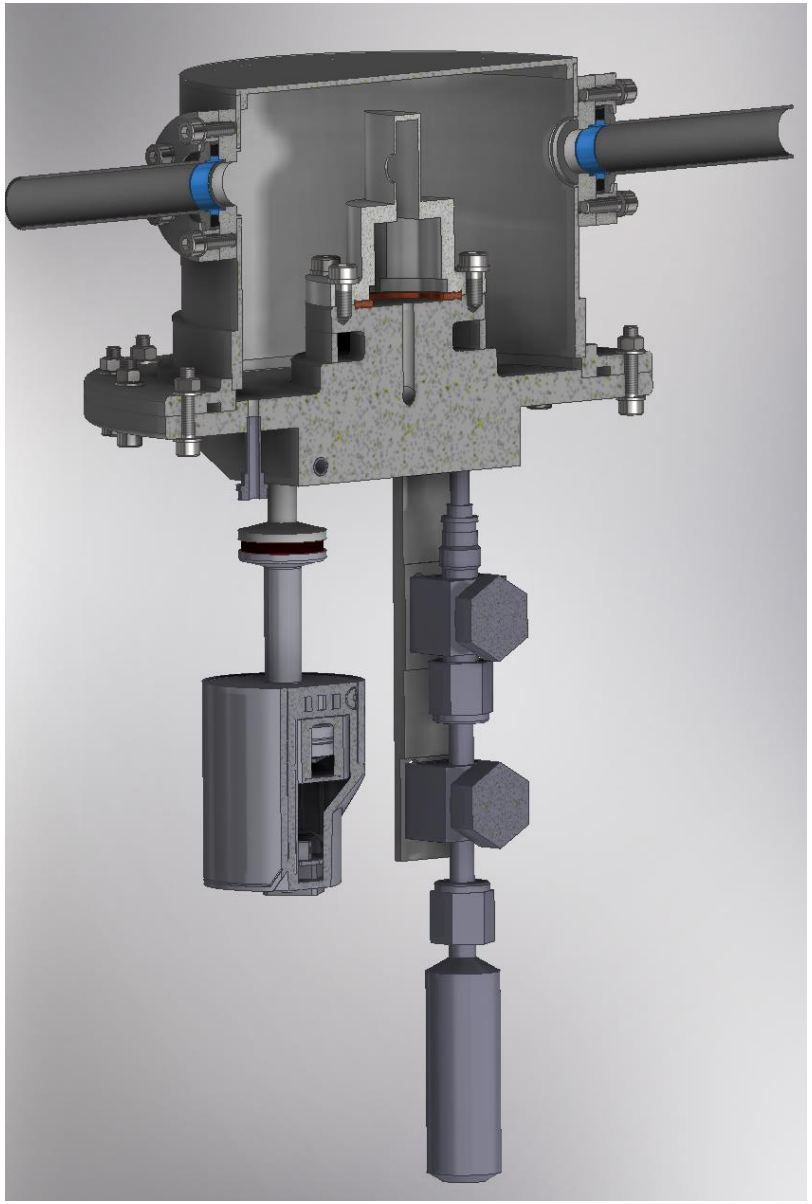

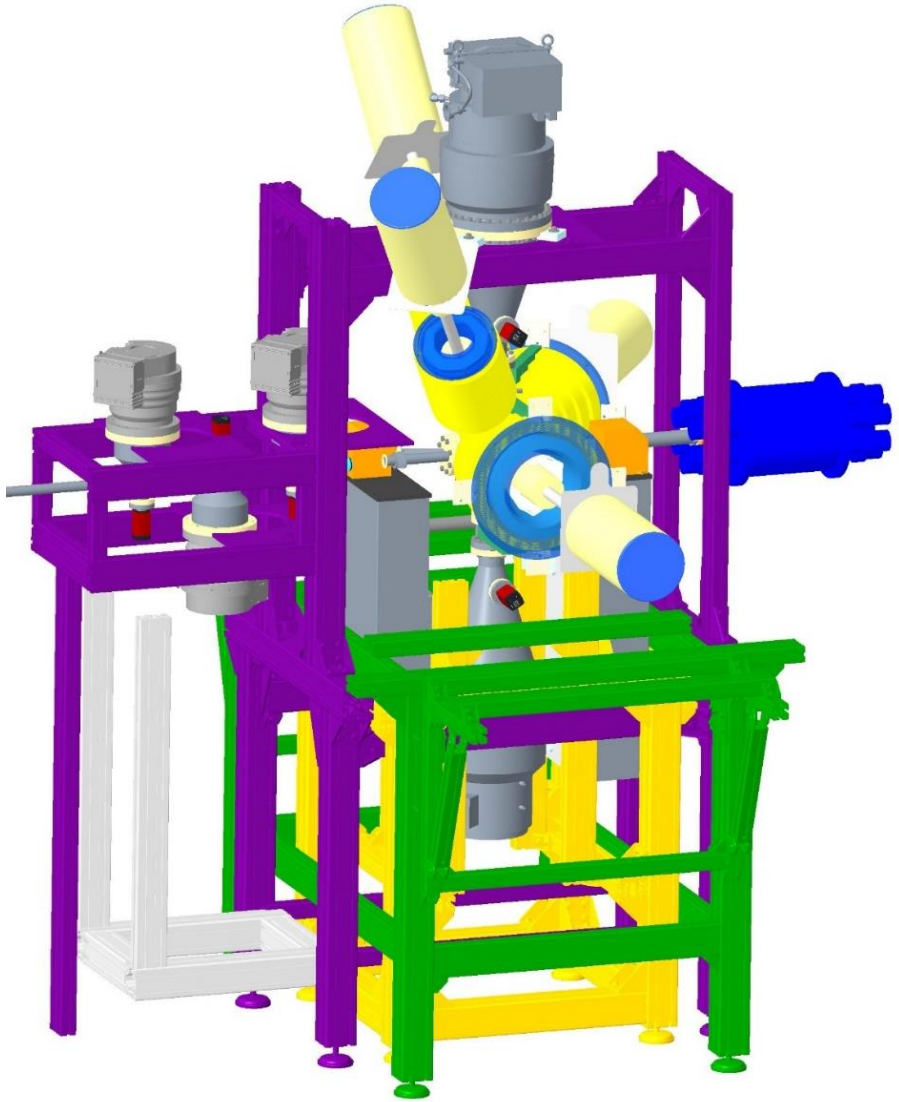

Thank you for your attention!